1977ApJ...214..268P

THE ASTROPHYSICAL JOURNAL, 214:268–299, 1977 May 15
© 1977. The American Astronomical Society. All rights reserved. Printed in U.S.A.

# PRODUCTION OF GAMMA-RAY BURSTS NEAR RAPIDLY ROTATING ACCRETING BLACK HOLES

TSVI PIRAN AND JACOB SHAHAM
Racah Institute of Physics, Hebrew University, Jerusalem
*Received 1976 August 26; revised 1976 November 1*

## ABSTRACT

A model for the production of $\gamma$-rays during the occurrence of instabilities in accretion of matter onto rapidly rotating black holes is described. Gamma rays are produced by Compton scattering of infalling X-ray photons, whenever the optical depth in the deep ergosphere is of the order of the gravitational distance. The initial photons are produced farther away by viscous processes in the infalling plasma, and contribute to the lower-energy regime of the burst spectrum, along with low-energy photons produced in the deep ergosphere. Calculated spectra for that specific Compton scattering may account for burst spectra in the range $\sim 300$ keV–3 MeV.

*Subject headings:* black holes — gamma rays: bursts

## I. INTRODUCTION

Since the first report on the discovery of $\gamma$-ray bursts (Klebesadel, Strong, and Olson 1973), numerous models have been suggested for their production. These models place the bursts at distances varying from solar system to extragalactic, and invoke astronomical systems of various sizes and nature. Some of them are summarized by Ruderman (1974); since this review, a few additional models have been put forth.

Some of the suggested models place the bursts near black holes. The physical processes in accretion disks around black holes have been worked out in some detail for steady-state accretion down to $r_{ms}$, the marginally stable Keplerian radius. This has been done with relation to X-ray emission from black holes in binary systems, and the single major mystery remaining is the nature of the microscopic viscosity.

This mystery is even more prominent when one is discussing nonsteady accretion extending, possibly, beyond $r_{ms}$ and all the way down to $r_{mb}$, the marginally bound radius (which represents the innermost possible perihelion–radial turning point—for particles with $E/\mu \lesssim 1$). Such accretion seems to be instrumental in $\gamma$-ray black hole models, and one must continue to make ad hoc assumptions regarding the viscosity for it.

In this paper, we wish to present fuller details for a model of which only a preliminary report has been published before (Piran and Shaham 1975*a*, *b*). The model we are suggesting associates $\gamma$-ray bursts with instabilities in accretion of matter onto rapidly rotating black holes, and differs from other models invoking black holes in one important aspect:

There is evidence (Cline and Desai 1975) that the observed $\gamma$-ray bursts, even though varying in direction, total energy, and temporal structure, do have very similar spectra above $\sim 300$ keV. In that energy regime, these spectra could be fitted by a tangent power law of index $-2.5$ (see Fig. 1). Our model associates this rather unusual feature of the constancy of the spectrum with Compton scattering of radially infalling photons by plasma, revolving at turning points deep in the ergosphere. When the optical depth is of the order of the gravitational distance, such scattering—which, for the higher-energy scattered photons, is a realization of the Penrose process (Penrose 1969)—produces, on the average, photons with energies around the electron mass. The spectra, when viewed by observers at infinity at varying angles from the equatorial plane, are either deficient in high-energy photons altogether or, when such photons are observed, have a characteristic energy dependence very similar to the observed power law. We note that, even though, in the local inertial frame, the process is a regular Compton process, an observer at infinity sees the photons gaining energy. We shall hence call it "inverse" Compton scattering.

Even though the infalling plasma does become quite hot, we suggest that its thermal radiation contributes only to the lower-energy regime of the observed bursts; for a certain time period during the instability, optical paths in the deep ergosphere become adequate for having "inverse" Compton conversion of some of this thermal radiation into nonthermal soft $\gamma$-rays, whose characteristic energy depends more on the mass of the electron than on the ambient temperature; hence the relative constancy of the spectrum.

The physical nature of the instability in the matter-accretion pattern, which our model requires, cannot be worked out in any great detail at the present level of understanding of the viscous mechanisms operating. Nevertheless, instabilities have been shown to exist, and our model is not too sensitive to their exact nature.

We have calculated numerically many such "inverse" Compton spectra for various temperatures of initial photons and plasma, various density and velocity profiles of the instability, and various observer



© American Astronomical Society • Provided by the NASA Astrophysics Data System

1977ApJ...214..268P



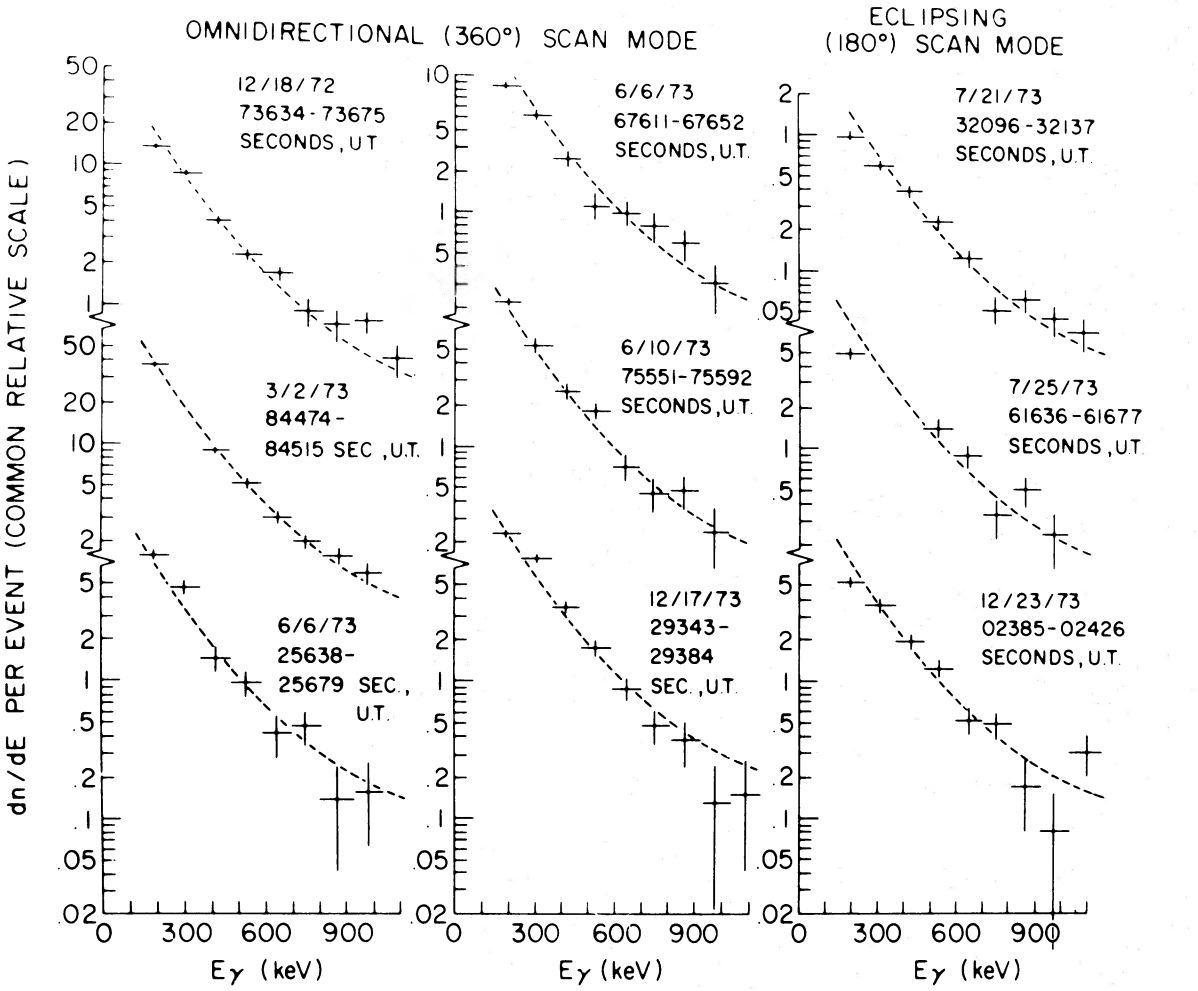


FIG. 1.—Evidence for single spectra of $\gamma$-ray bursts, from Cline and Desai 1975. These spectra were measured by IMP-7 for nine different bursts.

locations, for a "canonical" black hole ($a = 0.998\,M$). We present a few examples of the spectra, to be compared, on the one hand, with the observed spectra, and, on the other hand, with thermal spectra of suitable temperatures. The latter do not seem to have as good a fit with observations on the high-energy side.

The theoretical background for these computations has been summarized in another paper (Piran and Shaham 1977), hereafter Paper I; here, we concentrate only on the astrophysical results. Section II summarizes the "inverse" Compton-Penrose process, and is followed by a brief summary of the observations. Next, we present our suggested scenario, followed by a description of our results and plasma relaxation. Finally, we check our scenario against the other details of the observations; in particular, we show it to be not inconsistent with the possibility that Cyg X-1 is the origin of some of the bursts (even though any observational evidence for that is, so far, only circumstantial; Strong 1976).

## II. PENROSE PROCESSES AND "INVERSE" COMPTON SCATTERING

The Penrose process was first suggested by Penrose (1969) as a way to extract energy from a rotating black hole. According to this idea, a particle can disintegrate into two particles in the ergosphere of a rotating black hole in such a way that one of the resulting particles will have more energy (relative to an observer at infinity) than the original particle. The other resulting particle goes into a "negative energy" state and is captured by the black hole; hence the energy gain is shown to come from the rotational energy of the black hole.

Various calculations have shown that, even though the process in this original form is of great theoretical importance, it should not be expected to be very efficient in realistic astrophysical scenarios (Bardeen, Press, and Teukolsky 1972; Mashhoon 1973; Wald 1974; Kovetz and Piran 1975*a*, *b*; Paper I).

A different version of this process, the four-body

© American Astronomical Society • Provided by the NASA Astrophysics Data System

1977ApJ...214..268P



version, in which two particles collide to form two or more outgoing particles, was, however, shown to be potentially more efficient astrophysically (Piran, Shaham, and Katz 1975). The general theory for these processes was discussed in detail in separate papers (Piran and Shaham 1975*b*; Paper I).

Probably the most interesting example of the Penrose process occurs in the "inverse" Compton scattering, in which an infalling photon is scattered by an electron close to the horizon and gains energy from it. This effect is a basic ingredient of our model for $\gamma$-ray bursts, and we shall recapitulate its basic properties here, referring the reader to Paper I for details.

In general, the energies of the escaping photons, after "inverse" scattering in the equatorial plane, are around the rest energy of the electron ($\sim 500$ keV).

The reason for that is that, in the local inertial frame in which the electron is at rest (LBF of Paper I), the photon is extremely blueshifted, so that $h\nu \gtrsim \mu_e c^2$. Hence, in the LBF, the scattered photons have energies around $\mu_e c^2$. Some of them may not be redshifted again on escaping the infinity, as the rapidly rotating metric "assists" in their escape. The metric does so in an almost constant manner for all photons escaping at angles less than $\sim 45°$ to the equatorial plane. Higher-angle photons have much lower energies. As an example of high energy that a photon might acquire, we can use the maximal energy for an escaping photon after one special scattering, which we call the "canonical scattering" (scattering of a radially infalling photon by an electron which rotates in a circular orbit in the equatorial plane). This energy is $4.3\,\mu_e \approx 2.15$ MeV, for an extreme Kerr black hole and an $r_{\rm ms}$ electron, independent of the initial photon energy; this process is a Penrose process.

A small number of scatterings can raise this photon energy, but too many scatterings will cause thermalization of the spectrum. It should be noted that, throughout this paper, we shall call "thermal" any spectrum at infinity of photons which originate from any kind of local thermal equilibrium between photons and matter in a local inertial frame. Such thermal spectra at infinity reflect both the local temperature (thermal local energies) and the gravitational and Doppler frequency shifts (thermal random directions of local motion).

Even though a certain electron temperature is preferable for assisting in getting out more energetic scattered photons, one finds, in contrast with thermal photon-production processes, that the energy of the photons does not depend strongly on the electron temperature. It is the random velocities of the thermal electrons, rather than their thermal energies, that improve the Compton scattering process.

All of the resulting spectra have a nonthermal shape which is relatively independent of the details of the scattering configuration, and of other details of the scenario, over a wide range of possible scenarios. This property is of great importance and is confirmed by numerical calculations that we present below.

An important aspect of our suggested process is that it is most effective for photons which arrive at the scattering points with energies $\sim \mu_e c^2$; for these, efficiency will be highest, as they will already be energetic enough to be able to acquire sufficient energy from the electrons, and the Klein-Nishina cross section will not be much smaller than the Thomson cross section. Thus, for each configuration of plasma, $a/M$, and initial energies of free-falling photons, the scattering process will control itself, so that the electrons will locally gain similar energies in any scenario.

As mentioned before, for an isolated Compton-Penrose process, the scattered photon gets its energy from the scattering electron which, in turn, is captured by the black hole and appropriately reduces its rotational energy (Christodoulou 1970). The situation is more complicated when "inverse" Compton effects are taking place in a plasma surrounding the black hole. The infalling matter has three components, photons, electrons, and protons, and is likely to have an embedded turbulent magnetic field. The photons are scattered by the electrons, and, in a situation with maximal efficiency, the total energy with which the photons escape to infinity is of an order of magnitude of the total electronic rest mass, i.e., some (5–10) $\times$ $10^{-4}$ of the rest mass of the infalling matter. Normally, however, the electrons are not decoupled from the protons or the embedded field; these could exert a torque on the scattered electrons which were deflected into negative energy orbits, and bring them back to average positive energy orbits. Now these electrons can participate in more scattering, and the energy gained by the photons will come not only from individual electrons but from the infalling protons as well.

The energy available for the photons depends on the coupling between the electrons and the protons; in extreme cases, the photons could acquire all of the mass energy of the matter falling into the black hole. In the following discussion we shall present a simple model for estimating the coupling between the electrons and the protons and hence for calculating the efficiency of energy extraction from the infalling matter by impinging free-falling photons.

Thus, in contrast with the simplified case of isolated scattering, the photon energy in the realistic case is not gained from the black hole but dominantly from the rest mass of the infalling matter; the black hole serves as a suitable background metric for an efficient energy extraction, from this matter, by Compton scattering.

## III. OBSERVATIONS

Gamma-ray bursts were first observed in 1967 by the *Vela* satellites (Klebesadel, Strong, and Olson 1973). As of 1975 September, 56 bursts have been observed by these, by other satellites, and by experiments carried on balloons.

All the bursts are basically soft $\gamma$-ray bursts (a few hundred keV up to a few MeV) with some hard X-rays. The bursts have a unique nonthermal spectrum

© American Astronomical Society • Provided by the NASA Astrophysics Data System

1977ApJ...214..268P



which does not seem to vary much from one burst to another (Cline and Desai 1975), while their temporal structure varies greatly on all time scales from several seconds down to a few milliseconds. We shall summarize here the basic observational properties of these bursts, referring the reader to recent review articles for more details (Strong, Klebesadel, and Evans 1974, 1975).

*a) Energy Flux and Spectrum*

The energy flux on Earth of the observed bursts ranges between $10^{-4}$ and $10^{-6}$ ergs cm$^{-2}$. Weaker bursts are sometimes measured by balloon experiments (for example, Bewick *et al.* 1975).

Most of the energy of the flux is in soft $\gamma$-rays, with peak energy around 250 keV. The best measured spectrum could be fitted either by two power laws, $N(E) \propto E^{-1.38}$ below 300 keV and $N(E) \propto E^{-2.63}$ above 300 keV [$N(E)$ is the number of photons per energy interval]; the lower-energy part of the spectrum could also be fitted by $N(E) \propto e^{-E/(325\ \mathrm{keV})}/E$ (Metzger *et al.* 1974). There is complete agreement between this single spectrum, measured by *Apollo 16*, and the spectra measured by other satellites (Cline and Desai 1975; Wheaton *et al.* 1973).

Cline and Desai have shown that the spectra of all bursts are remarkably similar; the spectra measured by them in nine cases are shown in Figure 1. One can still observe small variations during the bursts; the $\gamma$-ray bursts seem to ride over a softer X-ray burst of a longer time span, and there is a rapid hardening of the spectrum in the beginning of the burst and a slow softening toward its end (Imhof *et al.* 1974; Palumbo, Pizzichini, and Vespignani 1974). The overall spectra have flat "tails" at high energies that extend up to a few MeV. The first of the above-mentioned analytic fits seems to reproduce this high-energy tail somewhat more accurately than the thermal one. There are no discrete lines in the $\gamma$- or X-ray spectra. Also, no optical or radio components have been found, so far, in correlation with the bursts (Grindlay, Wright, and McCrosky 1974).

*b) Temporal Structure*

There are around 10 burst observations per year. Some of the bursts appear in groups in which the interval between bursts is much shorter than average (Cline and Desai 1975). However, it is not proved that the distribution of time intervals between bursts is inconsistent with their occurring randomly (Strong, Klebesadel, and Evans 1974).

The duration of the individual pulses ranges between a few seconds to a tenth of a second. All the bursts show high temporal variability on short time scales, down to the resolution limit of the observational equipment. The detailed temporal structure of the bursts is far from constant, and there are variations between the temporal structures of various bursts.

*c) Direction and Spatial Distribution of the Sources*

The direction measurements of the pulses are quite poor. At the moment, no direction measurement is given for most of the bursts, and in cases for which there is such measurement, the error boxes are relatively large.

The galactic latitudes of the sources which have a known direction suggest that there may be a concentration of sources in the galactic plane (Strong and Klebesadel 1974). The sample of intensity distribution of the sources measured by the *Vela* satellites is not large enough to enable us to distinguish between sources distributed uniformly throughout a volume and sources distributed uniformly over a plane. Further measurements, which were carried out by balloons and by more sensitive satellites (Cline 1974; Bewick *et al.* 1975), suggest that the actual distribution is somewhere between the above-mentioned possibilities.

*d) Bursts from the Direction of Cygnus X-1*

There is some evidence of connection between a few of the $\gamma$-ray bursts and the X-ray source Cyg X-1 (Strong 1976). The reported error box for the direction of the source of burst 72-2 contains Cyg X-1, which is about 1° from its center. This burst lasted 6 s, and its total energy flux was $10^{-5}$ ergs cm$^{-2}$. The reported error box of burst 71-2 also contains Cyg X-1, which is 3° from the center. (The error box of this burst is very large, owing to observational difficulties.) Like burst 72-2, 71-2 lasted about 6 s and its total flux was $10^{-5}$ ergs cm$^{-2}$; it occurred on 1971 March 15, around the same time that Cyg X-1 was going through a change in its X-ray spectrum and intensity; the latter change occurred during 1971 March–April (Tananbaum *et al.* 1972).

A few other bursts, from unknown directions, occurred on 1975 April 22 and 26 and had similar duration and intensity. During that same period, Cyg X-1 was having another change in its spectrum and intensity. It is reasonable to assume that there is some connection between the X-ray source Cyg X-1, in particular changes in it, and some of these $\gamma$-ray bursts.

The bursts 72-2 and 72-3 (which have unidentified directions but have similar duration and intensity) did not coincide with any observed change in the spectrum of Cyg X-1. However, as Sanford *et al.* (1975) have pointed out, Cyg X-1 was not monitored continuously during 1972, and it is possible that changes which lasted less than a month have occurred but have not been noticed.

Finally, as Ruderman has pointed out (Ruderman 1974), the X-ray emission from Cyg X-1 contains many small bursts which last about half a second and are composed of millisecond pulses. These small bursts have very irregular temporal structure that resembles the temporal structure of the $\gamma$-ray bursts, and one may wish to associate them with a common mechanism.

## IV. SCENARIO FOR GAMMA-RAY BURSTS

According to the model which we present (Piran and Shaham 1975*a*, *b*), "inverse" Compton scattering deep in the black hole ergosphere plays a dominant

© American Astronomical Society • Provided by the NASA Astrophysics Data System

1977ApJ...214..268P



role in producing the $\gamma$-rays above 300 keV in the bursts. "Inverse" Compton effects also contribute to the softer part of the spectrum, but in this region, a large part of the radiation is produced by bremsstrahlung and Comptonization processes which are taking place in the hot plasma farther away (Lightman, Rees, and Shapiro 1975).

The necessary conditions for an efficient "inverse" Compton scattering can be fulfilled in the ergosphere of a black hole which is a part of a binary system. When there is a mass transfer between the normal star and the black hole, the matter is falling onto the black hole through an accretion disk. The $\gamma$-ray events can be triggered by a matter flow instability in such a disk, which results in the collapse of the inner region of the disk and in the appearance of optically thin plasma deep in the ergosphere, with turning points there.

Binary systems which contain a black hole as a member were suggested in 1966 (Novikov and Zel'dovich 1966; Shklovsky 1967) as possible sources for X-rays. In such systems, the matter passing from the normal star settles down in form of a disk in order to get rid of its surplus angular momentum. This angular momentum is transferred outward by viscous processes which also heat the plasma up; the excess energy is emitted as X-ray radiation. Pringle and Rees (1972) and Shakura and Sunyaev (1973) were the first to discuss the structure of Newtonian disks. Novikov and Thorne (1973) and Page and Thorne (1974) extended these ideas for relativistic disks around rotating black holes. Since then, a great deal of work has been done on disk structure, and a recent review on this subject was written by Lightman, Rees, and Shapiro (1975).

We shall briefly summarize a few properties of these disks that are important for the discussion of our model.

1. The disk can be divided into three regions: an outer region, in which the gas pressure and free-free scattering are dominant; an intermediate region, in which gas pressure is still dominant but the opacity is mainly due to electron scattering; and an inner region, in which photon pressure and electron scattering are dominant.

2. The gradient of the gravitational potential energy becomes larger, and hence both the energy-production rate and the temperature grow, as the plasma gets near to the horizon. Owing to this high temperature and high energy-production rate, the inner region of the disk is optically thin (Thorne and Price 1975), secularly unstable (Lightman and Eardley 1974; Lightman 1974*a*, *b*), and thermally unstable (Pringle, Rees, and Pacholzyk 1973).

3. Under steady-state conditions, the plasma in the disk moves slowly inward in almost Keplerian orbits. The matter reaches $r_{ms}$, and free-falls quickly into the black hole from this radius. Clearly, the inner region of the disk ends at $r_{ms}$, and the density of matter inside $r_{ms}$ is relatively very small.

4. At the moment, it is not clear what is the exact mechanism of viscosity in the disk. Molecular viscosity is not sufficient to account for the rates of energy production and angular momentum transfer which are observed in the known X-ray sources. The common assumption is that the viscosity is well-developed magnetic and/or turbulent viscosity.

5. In some configurations, the mass transfer is due to Roche lobe overflow. In other cases, the accretion is in the form of stellar wind accretion. In the latter instances, the matter may have only a marginal amount of the angular momentum needed for disk formation (Illarionov and Sunyaev 1975; Shapiro and Lightman 1975). In Cyg X-1, for example, the accretion process is most likely a stellar wind–type rather than Roche lobe overflow, as the primary seems to fill its Roche lobe only to 98% (Tananbaum and Hutchings 1974). This is also in agreement with theoretical calculations of van den Heuvel (1975), according to which Roche lobe accretion could not exist in Cyg X-1, since it would have resulted in too high a rate of mass transfer.

Before going into the discussion of scenario during an instability, we shall point out that, in steady state, the optical path in the inner ergosphere is very small. The optical path $\tau$ between $r_{ms}$ and $r_{mb}$ is

$$\tau = \int_{r_{mb}}^{r_{ms}} \kappa \rho dr_p ,$$

where $\kappa \approx \kappa_{es}$, $\rho$ is the proper matter density, and $dr_p$ is an element of proper distance. Denoting by $\dot{m}$ the mass accretion rate and assuming that this mass falls in anisotropically, with about the velocity of light, through a surface area which is approximately $2\pi r_g^2$, we can estimate $\tau$ to be

$$\tau = \frac{1}{2\pi r_g^2 c} \int_{r_{mb}}^{r_{ms}} e^{\mu_1} dr , \qquad (1)$$

where $r_g$ is the gravitational radius and $e^{\mu_1}dr$ is the proper distance element. Relating $\dot{m}$ and $L$, the total luminosity, by $\dot{m} = L/\eta c^2$ ($\eta$ is the efficiency parameter which is of order 0.1, $0.05 \leq \eta \leq 0.4$), and evaluating the proper distance between $r_{ms}$ and $r_{mb}$ to be of order $r_g$ for an $a/M = 0.998$ black hole, we have:

$$\tau \approx 20 \frac{L_{38}}{M} . \qquad (2)$$

$L_{38}$ is the luminosity in $10^{38}$ ergs s$^{-1}$ and $M$ the mass of the black hole in units of solar masses. Furthermore, under steady-state conditions, the plasma beyond $r_{ms}$ is likely not to have any turning points and is falling in essentially radially. No efficient "inverse" Compton scattering of infalling photons occurs under these circumstances, and any outgoing scattered photons will be quite soft X-rays (Shapiro 1974; Paper I).

One may conclude that even though there is a copious flow of photons with energy above 10 keV in the inner ergosphere, most of them are not scattered at all; and in steady state, very few Penrose processes are taking place.

However, a large amount of tangentially moving plasma may appear temporarily in the inner ergosphere during a period of instability in the disk. Also, in such

© American Astronomical Society • Provided by the NASA Astrophysics Data System

1977ApJ...214..268P



cases, the plasma density in the ergosphere can be much larger than the steady-state density; hence, "inverse" Compton scattering should occur. One should remember that the inner region of the disk is indeed sensitive to various instabilities, which may be triggered by one or more of the following factors:

1. Sudden overflow of the Roche lobe of the primary (caused by a flarelike process) may result in an enhanced rate of accretion onto the black hole. This mechanism can be of importance in the cases of Roche lobe accretion and of stellar wind accretion, mostly whenever the Roche lobe is "almost" filled.

2. There may be changes in one of the parameters of the stellar wind (direction, density, etc.), in a configuration with stellar wind–type accretion. In such a case, it may become possible that the direction of rotation of the disk will reverse (Shapiro and Lightman 1975). Owing to the difference between the $r_{ms}$ values for retrograde and prograde motion, this process results in large changes in the inner disk structure, especially in the region between the two $r_{ms}$ values; this region is either filling up or emptying.

3. A Lightman-Eardley instability or a thermal instability may develop which is not connected directly with changes in the mass-transfer mechanism.

In the first and the second possibilities, the disk passes from one stable state to another through a period of instability and rearrangement. In the third, the disk is normally only in a marginally stable equilibrium, and any small excitation triggers the instability, after which the disk returns to the same marginally stable configuration.

It is clear that one should expect a large infall of matter into the ergosphere during the rearrangement of the disk toward its new configuration, especially in case of inversion of the direction of rotation of the disk. If the angular momentum of the infalling plasma is small but not zero, which is the realistic case, the plasma will move in highly eccentric elliptical orbits with perihelia deep in the ergosphere, down to the $r_{mb}$. This is because most of the Keplerian orbits in the region in question do have $E \sim \mu$. Owing to the viscous processes, the plasma will fall gradually into the hole, forming, perhaps, quasirings during its inward motion (Mészáros and Rees 1975).

The infalling matter will heat up during these processes. It is reasonable to assume that the electrons will reach temperatures around $10^9$ K (see, Shapiro, Lightman, and Eardley 1976; and the numerical calculations below). Since the optical distance is of order unity and more, the matter will mainly emit bremsstrahlung radiation [$N(E) \propto e^{-E/KT}/E$] around a few tens to a few hundred keV. Part of this radiation will escape the black hole and will contribute to the lower part of the burst spectrum. Another part of this radiation, which is formed outside of the horizon but falls inward, toward the black hole, will be "inverse" Compton scattered (in almost "canonical" processes) by the electrons in the plasma, which are now near their inner turning points. The emitted photons will have energies between a few hundred keV to a few MeV relative to an observer at infinity, and will be the dominant contributors to the upper part of the spectrum.

The bremsstrahlung functional behavior, which we have described for the low-energy region, roughly resembles one of the suggested analytic fits of Metzger *et al.* (1974) cited in the previous section. However, as we mentioned there, this fit does not seem to reproduce the high-energy portion too well, as it falls off too rapidly there. This is the general property of any attempt to describe the spectra by a thermal spectrum. Again, we suggest that bremsstrahlung is relevant only for the lower-energy part of the spectra.

For a complete analysis of this model, one needs a full description of the viscosity mechanisms occurring in the inner disk region, since these mechanisms will have an essential role in determining the details of the instability. We should point out that there is no need for viscosity different from that assumed for the various steady-state models for the disk.

One common assumption (see, for example, Lightman, Rees, and Shapiro 1975) is an ad hoc relation for the viscous stress, $t_{\phi r} = \alpha p$, where $t_{\phi r}$ is the $\hat{\phi}\hat{r}$ component of the energy-momentum tensor, $p$ is the pressure, and $\alpha$ is a numerical coefficient smaller than unity. Since the viscosity is mainly magnetic and turbulent viscosity, $\alpha$ may be written as (Shakura and Sunyaev 1973)

$$\alpha = \frac{v_T}{c_s} + \frac{B^2}{8\pi p}, \tag{3}$$

with $B$ standing for the magnetic field, $v_T$ for the turbulent velocity, and $c_s$ for the speed of sound. Assuming that there is a magnetic field in the rotating plasma and that the viscosity is really a magnetic viscosity, we shall note that under such conditions the plasma will move in blobs which are held together by their magnetic field. In these blobs, the magnetic force is balanced by the gravitational tidal force (Lightman, private communication), and the size of each blob, $l$, is determined by equating these forces; this yields

$$l \approx r_g \frac{v_A}{c} \approx r_g \alpha^{1/2} (c_s/c). \tag{4}$$

Here $v_A$ is the Alfvén speed. For accepted $\alpha$ values, which are around 0.1, this equation gives $r_g/50$–$r_g/100$ for the radius of a typical blob, which is of the order of a few hundred meters.

The plasma which is falling in magnetic blobs, or otherwise, will not fall at a constant rate. Owing to this variability, the optical path inside the ergosphere will vary between values which are either too high or too low for efficient Penrose processes. Hence there will be variations in the signal during the burst: In some moments, the process will be very efficient; in other moments, the signal will go down to zero. The time scale of changes will be of the order of light travel time over one blob. As we shall show in the next section, variations by a factor of 10 in the density of matter will carry the system from too low to too high optical depths.

© American Astronomical Society • Provided by the NASA Astrophysics Data System

1977ApJ...214..268P



## V. MODEL CALCULATIONS OF "INVERSE" COMPTON

In Paper I we described a method for calculation of the spectrum of escaping photons after "inverse" Compton scattering in the ergosphere of a Kerr black hole. These numerical calculations are performed using a computer code based on the Monte Carlo method. The calculations are more complicated than the usual radiation transfer computations, since the trajectory of the photon in its motion in the ergosphere is a null geodesic in curved spacetime, and both the trajectory and the optical path along it should be numerically integrated separately for each photon. Evaluation of the new photon parameters after a scattering includes the transformations between three coordinate frames: the LBF, in which the electron is at rest and in which the differential cross section is given by the Klein-Nishina formula; the Boyer-Lindquist coordinates, which are used to describe the motion of the photon in the Kerr metric; and the locally nonrotating frame (LNRF) (Bardeen, Press, and Teukolsky 1972), which serves as a convenient local inertial frame which is intermediate between the two coordinate systems.

The spectrum of escaping photons depends on the following parameters: The spectrum of the impinging photons $f_{\rm ph}(E_{\rm ph}, L_{\rm ph}, Q_{\rm ph})$, the density $n_e(r, \Theta)$ of electrons and their velocity distribution $f_e(\boldsymbol{P}_e, r, \Theta)$, the $a/M$ value for the black hole, and, finally, the angle of the observer at infinity relative to the equatorial plane.

As was already pointed out, it is difficult to describe the needed distributions without a reasonable model for the instability process and the viscosity mechanism. Lacking such knowledge, we used a simple model, based on ad hoc assumptions, to estimate the density distribution of the electrons in the ergosphere. Before going into the details of this model, we should stress that, as we shall shortly show, the resulting spectrum is found to be quite insensitive to the details of the density distribution. It is therefore hoped that the various assumptions lying behind these calculations will not greatly affect the realistic spectrum.

We have assumed that the instability develops at the boundary between the inner region and the intermediate region of the disk, i.e., close to the black hole but outside the ergosphere, at $r \approx 6$–$10\, r_g$ (Lightman 1974*a*, *b*). The matter loses its angular momentum in an abrupt manner (owing, say, to collision with matter rotating in the opposite sense) and falls in elliptic orbits. Owing to their thermal velocities, the particles fall into the ergosphere in various orbits around some average orbit. We first assume that the motion of the particles can be described by a geodesic motion (the particles are not influenced much by viscosity during their motion far from the horizon). After they get inside, we define small-volume elements around various points in the ergosphere to represent, for example, magnetic blobs, and assume that in these small elements the viscosity becomes suddenly maximal (Lin and Pringle 1975): All the particles in such a small-volume element are assumed to move with thermal velocity around their mean velocity, while the temperature is determined in such a way that the particles now have a thermal energy which is equal to their previous total kinetic energy in the center-of-mass frame of the volume element.

The viscosity in our model is, thus, a sum of delta functions. This very simplified model should be close to the realistic situation when the viscosity is magnetic and when the plasma is contained in magnetic blobs. In such a case, it is probable that the viscosity will indeed be strongest at points of field-line reconnection.

The distributions that result from such viscosity mechanisms were calculated, using a second computer code which is also based on the Monte Carlo method. In these calculations, we fix the initial point at the large distance at which the "infall" begins, the average energy, angular momentum, and $Q$ value (and hence the average orbit), and we also fix the initial temperature at that point. We choose a particle and pick a thermal velocity for it; hence its initial energy and momentum are determined. The geodesic motion of the particle is integrated and its contribution to various small-volume elements is cataloged. The calculations are repeated for many particles, and when the integration over all particle geodesics is terminated, the density, average momentum, and temperature are calculated for each volume element. Clearly, one calculates by this procedure only the relative density among the various volume elements: The density calculated at each point depends linearly on the total number of particles which are used in the Monte Carlo calculations. The "real" density which we relate to this result depends on the accretion rate, and is determined by an arbitrary multiplicative factor.

An example of density and temperature profiles which were calculated by this method in the equatorial plane is presented in Figure 2. Almost all the distributions which we have calculated have the following common features: The inward radial velocity of matter increases as we approach $r_{\rm ph}$, and the angular-momentum-to-energy ratio decreases. Note that, since the region below $r_{\rm ph}$ is not important for the spectrum calculations, all the distributions were evaluated only down to $r_{\rm ph}$. The density usually peaks around $r_{\rm ms}$ and falls off toward higher and lower $r$ values, while the temperature increases all the way down to $r_{\rm ph}$. The radial density profile does not change much when the initial temperature is increased; however, the angular distribution relative to the equatorial plane becomes broader, and the temperature inside is higher.

Apart from spectrum calculations for our calculated distributions, we have also calculated spectra for a few cases in which we used "arbitrary" density, temperature, and velocity distributions. These were added in order to investigate the influence of various factors on the "inverse" Compton spectrum. The "arbitrary" distributions include a few instances in which the electron density and temperature are constant throughout the ergosphere between $2\,M$ and $r_{\rm mb}$ and between angles of $\pm 10°$ from the equatorial plane, for a number of optical depths; one case of constant density and temperature in a wider range of

© American Astronomical Society • Provided by the NASA Astrophysics Data System

1977ApJ...214..268P



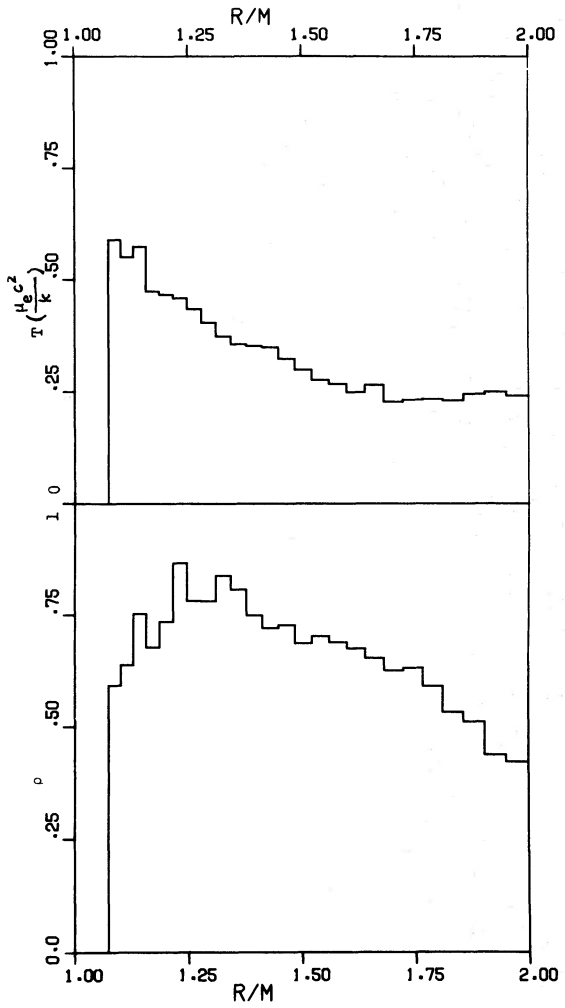


FIG. 2.—Calculated density and temperature distributions of the electrons in the equatorial plane, around a canonical black hole ($a/M = 0.998$). The initial point is $6\,M$ and the thermal velocity there, $v_T$, is $0.17\,c$. The parameters of the average orbit are $E = 0.99\,\mu_e$, $L = 2.09\,\mu_e M$, and $Q = 0$, representing an elliptical orbit with a perihelion close to $r_{mb}$. The various distributions are calculated only for $r > r_{ph}$ ($\equiv 1.074\,M$).

Other calculated distributions have similar features, except for a higher temperature profile when the initial temperature is higher. The density distribution has arbitrary units and extends to $\pm 20°$ from the equatorial plane. The temperature is measured in units of $\mu_e c^2$.

angles, $\pm 30°$ from the equatorial plane; and a few instances with constant density and temperature in the inner ergosphere, i.e., between $r_{ms}$ and $r_{mb}$. In all the above-mentioned cases, the velocity distribution was determined by the demand that the electrons move in circular orbits. (Note that spectra resulting from scattering by model rings were discussed in Paper I.)

In all cases, we have chosen the initial distribution of the photons, $f_{ph}$, to be a plane distribution with $T_{ph} = 50$ keV. In the one instance for which $T_{ph} = 25$ keV, Figure 3*g*, not much has changed. In so choosing, we have made use of the results of Paper I, in which we saw that the outgoing spectrum does not change much when $f_{ph}$ is varied. The $a/M$ value of the black hole was fixed to be 0.998, since for low $a/M$ values the process is clearly inefficient, while when the black hole has a higher $a/M$ value, it will very quickly settle down to this canonical value (Thorne 1974).

The resulting spectra are presented in Figures 3*a* to 3*r*. In each figure we plot the total emitted spectrum integrated over all angles, and five spectra at five observer angles relative to the equator. The error bars which appear in these figures are due to the statistical error of the Monte Carlo calculations, and do not include other possible errors which are due to uncertainties in the input data ($n_e, f_e, f_{ph}$, etc.).

In order to compare the calculated spectra with the observed ones, we have reproduced, in Figure 1, the experimental spectra. As was pointed out before, our spectra are quite insensitive to a wide range of variations in the details of the various distributions; and generally, most of the resulting spectra are quite similar to the observed spectra, which seem not to vary as well. When comparing the calculated and the observed data, one should remember that, in addition to "inverse" Comptonization, bremsstrahlung is an important contributor to the low-energy side of the burst spectra, and only the higher-energy part of the spectrum presented in Figure 3 should be used in forming such a comparison.

Most of the photons, carrying most of the energy, are emitted in angles less than $\sim 45°$ from the equatorial plane. In the region between 10° and 45° (outside of the disk but at small angles from the equatorial plane), there are only small angular variations in the spectra. The spectrum quickly becomes softer when the angle of the observer is increased, above 45°.

The first spectra, Figures 3*a*–3*g*, were calculated using the distributions presented in Figure 2, which are probably close to realistic ones. The angular distribution of electrons in this case is quite narrow; most of them lie inside of $\pm 20°$ from the equatorial plane. The electron energy and angular momentum are around $0.9\,\mu_e$ and $1.9\,\mu_e M$, respectively. The overall optical depth in the ergosphere was changed by multiplying the density distribution by various factors, and it was varied between $\sim 0.1$ and $\sim 12$ (this is the depth for an average initial photon; note that the optical depth for a scattered photon is usually higher). The optically thin cases are plotted first, and the thicker ones follow.

The shape of the spectrum does not vary much when the optical depth is increased from $\sim 0.1$ to $\sim 6$ (Figs. 3*a*–3*e*), even though a slight decrease in the high-energy regime can be noticed at the higher optical depth. The average number of scatterings (per one scattered initial photon) increases from one to four when the system goes from optical depth of 0.1 to 6. The most efficient process is seen to take place when the optical depth is around 3. In this case, a photon undergoes an average of 2.2 scatterings before it escapes or is captured by the hole. Note that in this case the optical depth is sufficiently high, and only 7% of the initial photons are captured by the black hole

© American Astronomical Society • Provided by the NASA Astrophysics Data System

1977ApJ...214..268P

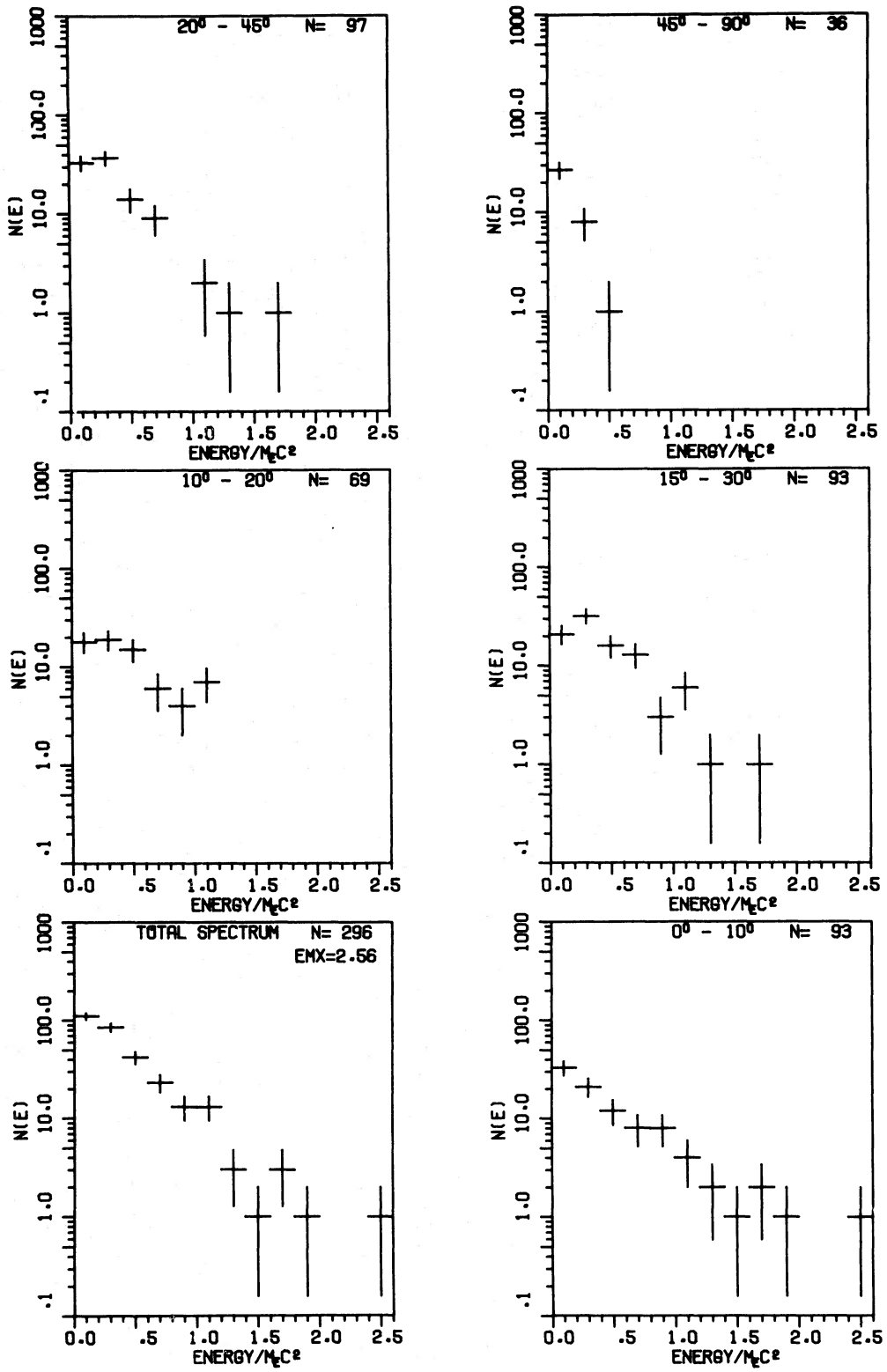


FIG. 3*a*

FIG. 3.—Spectrum of escaping photons after an "inverse" Compton scattering from various electron distributions.

The distributions are characterized by the density, temperature, and velocity distribution of the electrons, the initial photon temperature, and the optical depth for an initial average photon.

All the calculations were done for a canonical black hole.

In each figure the total spectrum, integrated over all observer angles, along with five spectra observed at various angles, is presented. The maximal energy for each case and the total number of escaping photons are printed on the figures.

The various parameters which describe the configurations for which the spectra were calculated are given in Table 1.



© American Astronomical Society • Provided by the NASA Astrophysics Data System

1977ApJ...214..268P

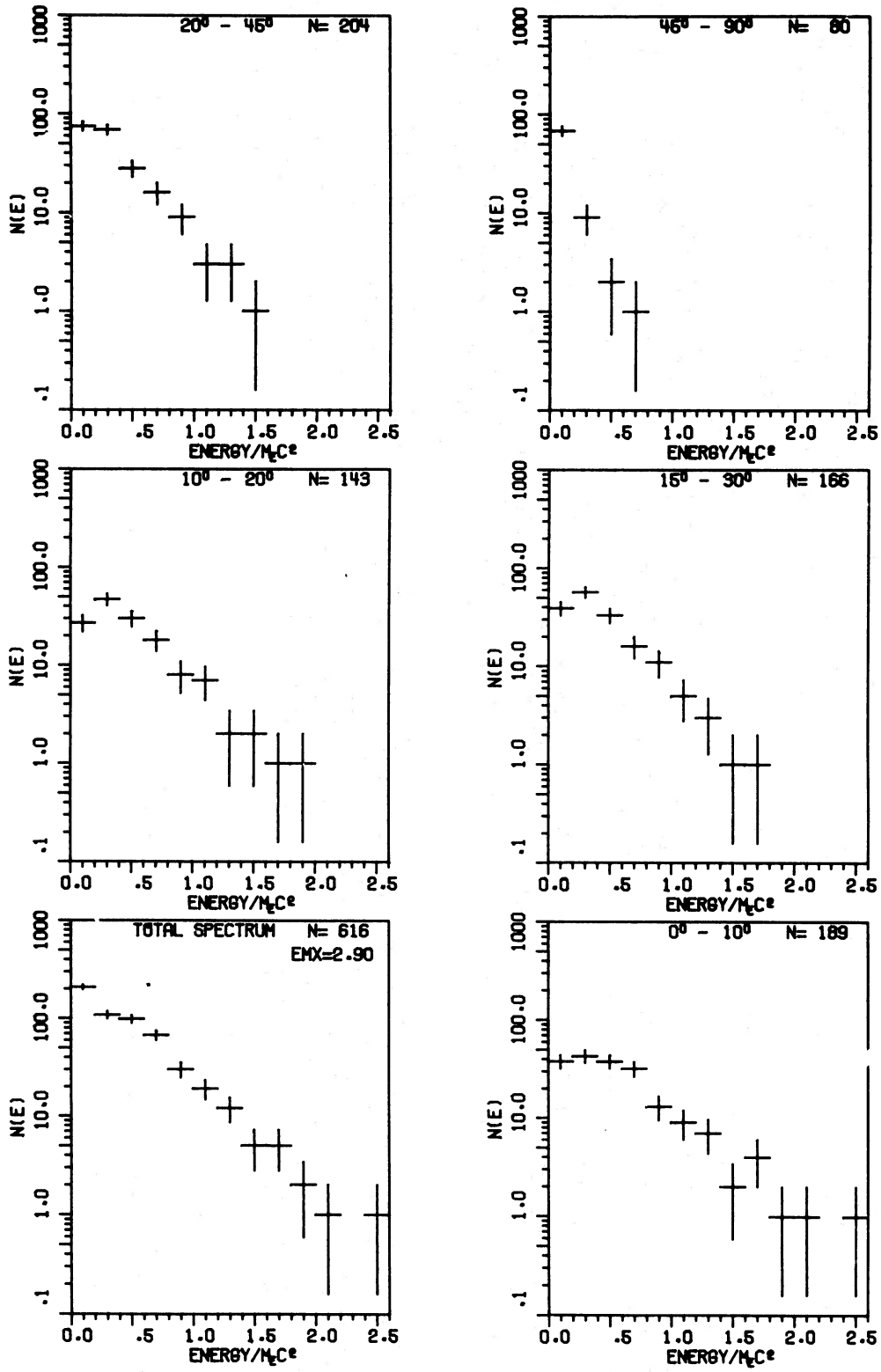


FIG. 3*b*

FIG. 3.—*Continued*



© American Astronomical Society • Provided by the NASA Astrophysics Data System

1977ApJ...214..268P

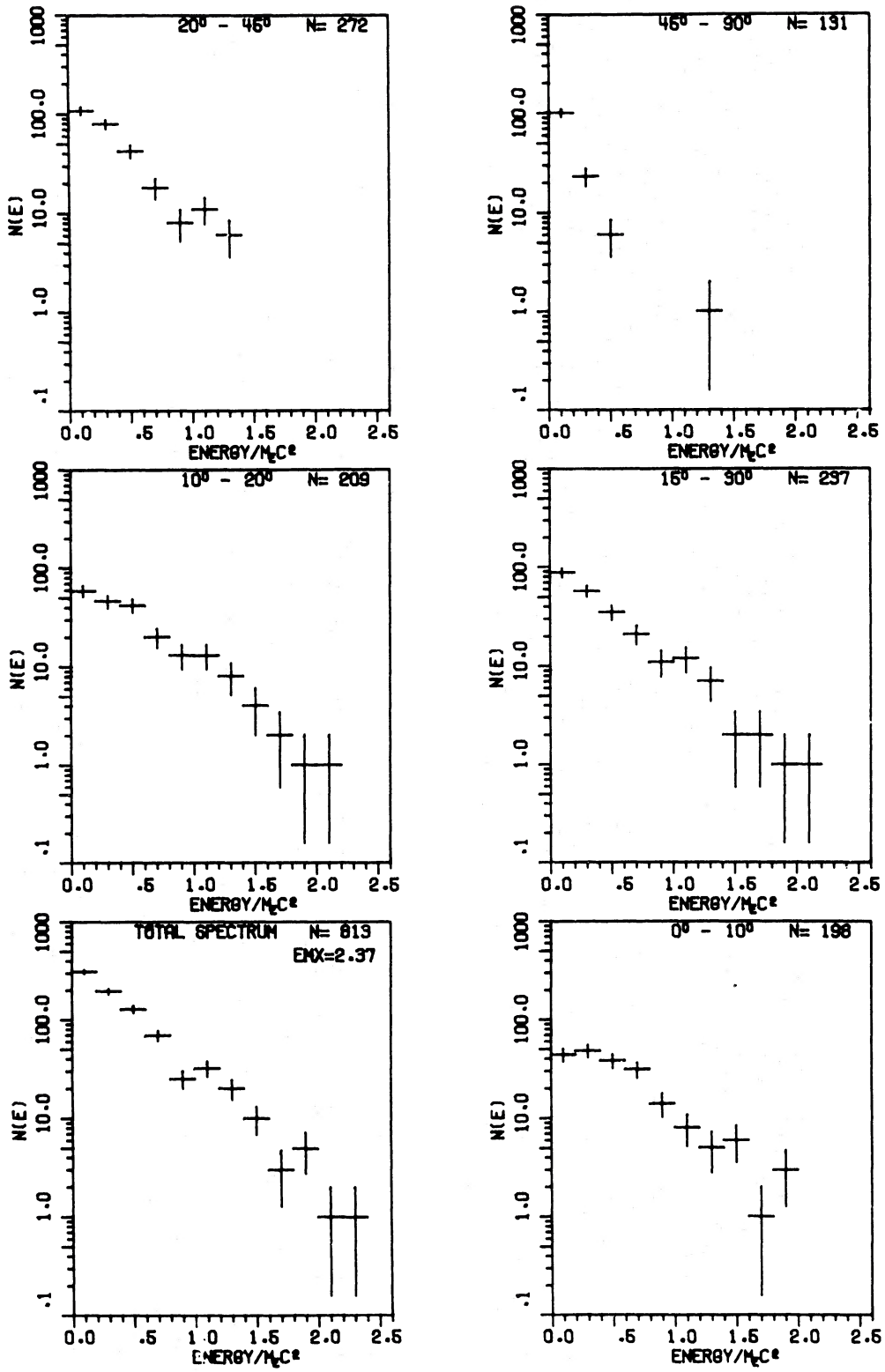


FIG. 3c

FIG. 3.—*Continued*



© American Astronomical Society • Provided by the NASA Astrophysics Data System

1977ApJ...214..268P

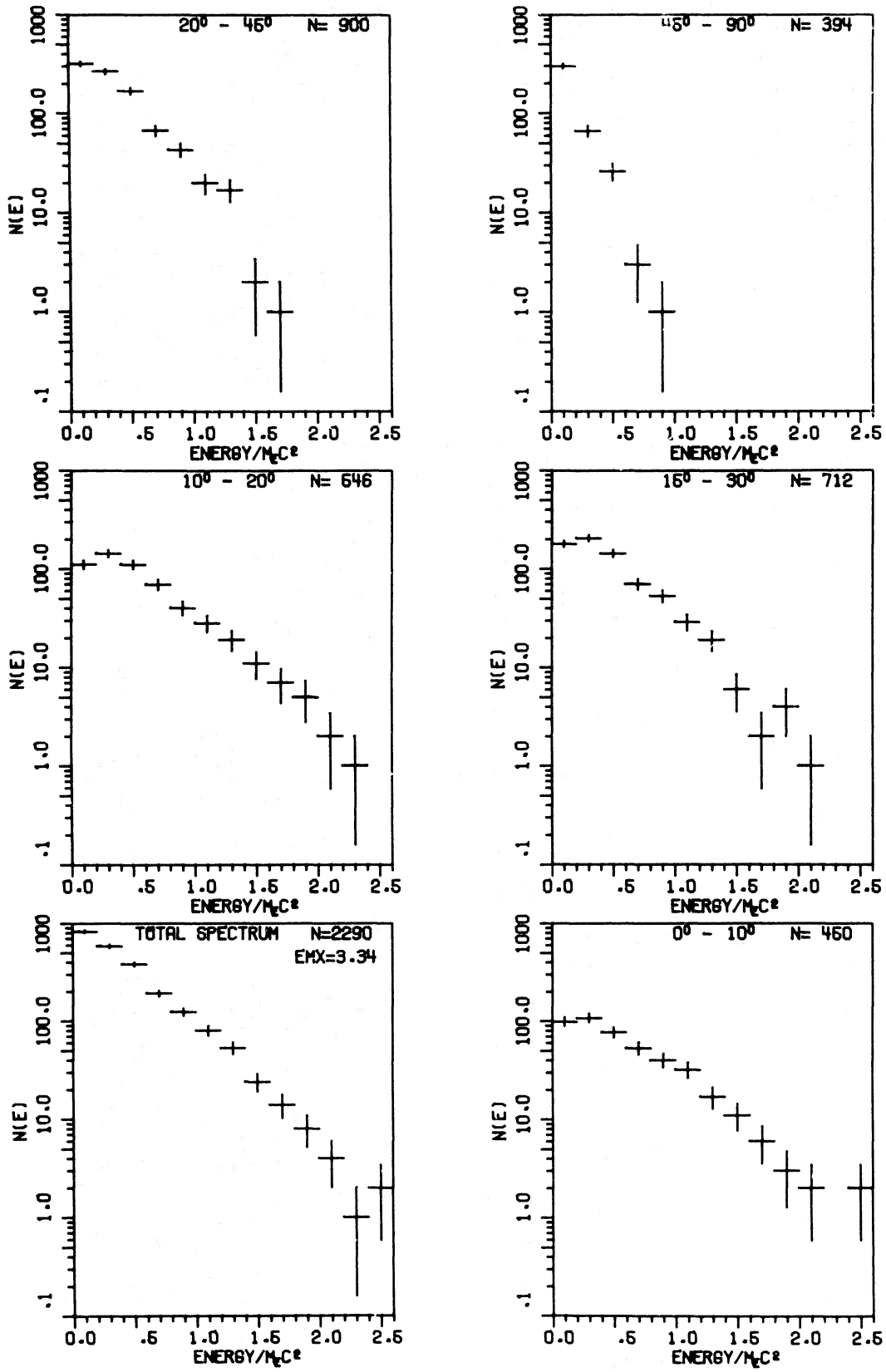


FIG. 3*d*

FIG. 3.—*Continued*



© American Astronomical Society • Provided by the NASA Astrophysics Data System

1977ApJ...214..268P

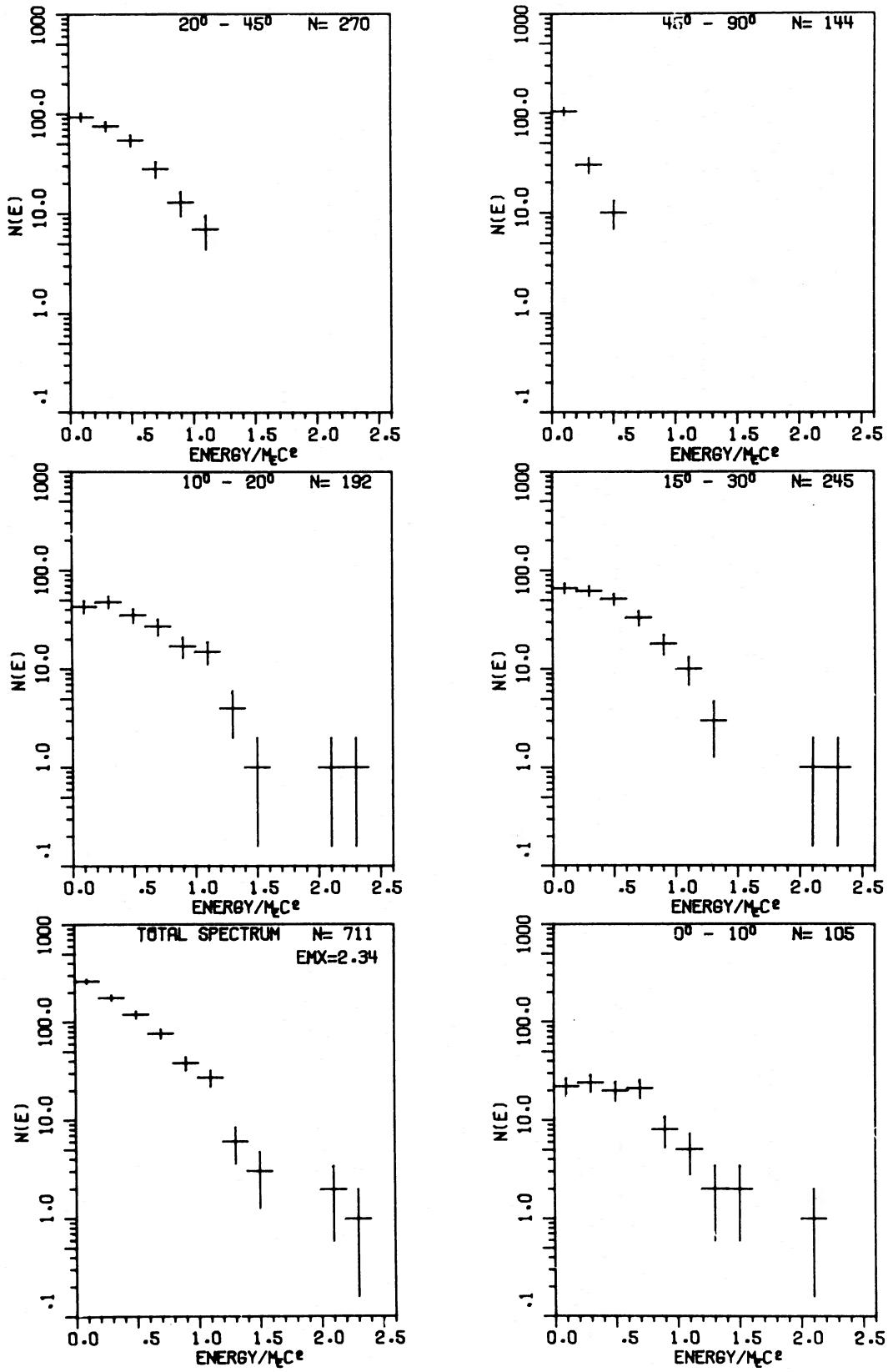


FIG. 3*e*

FIG. 3.—*Continued*



© American Astronomical Society • Provided by the NASA Astrophysics Data System

1977ApJ...214..268P

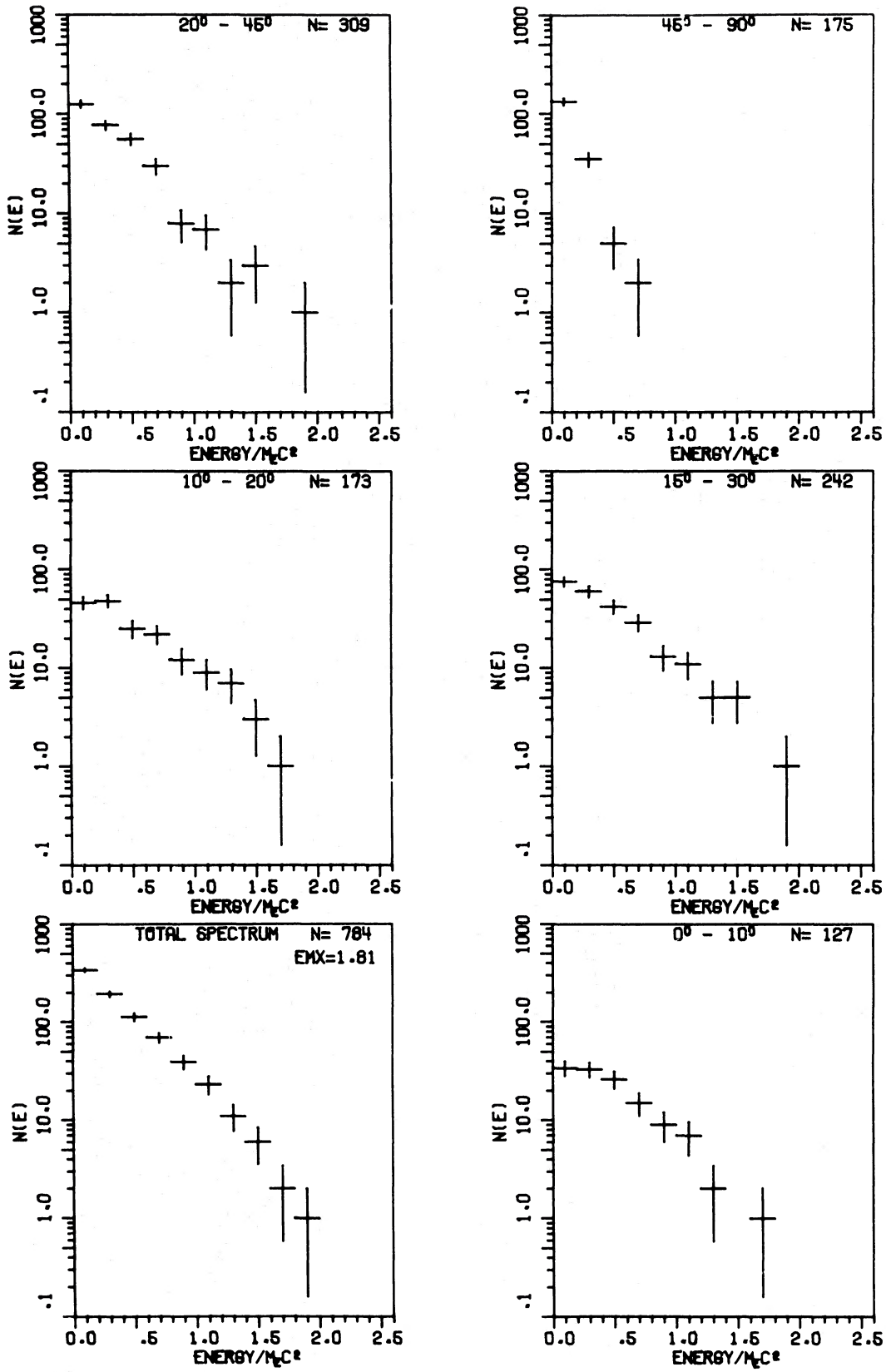


FIG. 3*f*

FIG. 3.—*Continued*



© American Astronomical Society • Provided by the NASA Astrophysics Data System

1977ApJ...214..268P

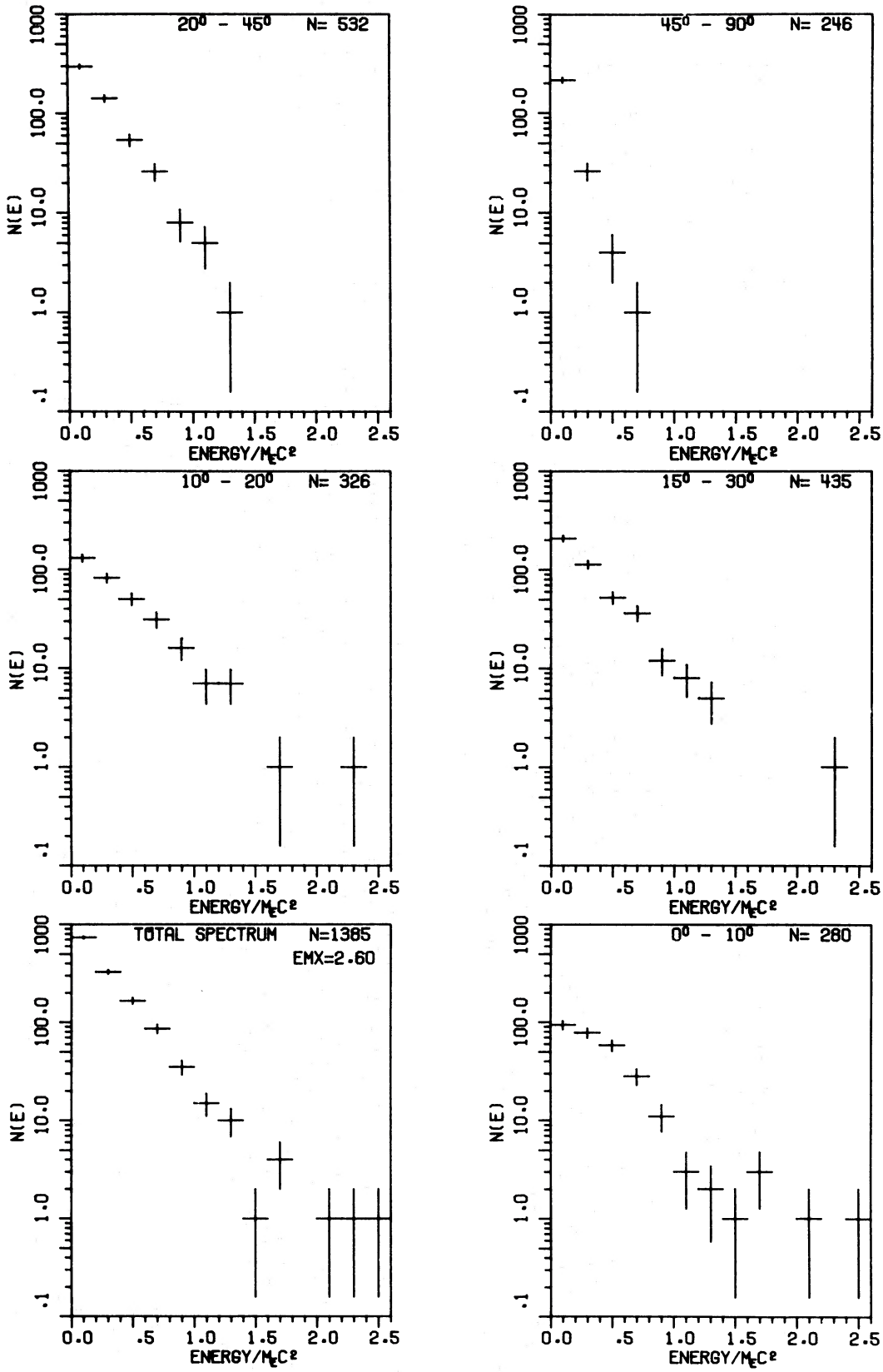


FIG. 3*g*

FIG. 3.—*Continued*



© American Astronomical Society • Provided by the NASA Astrophysics Data System

1977ApJ...214..268P

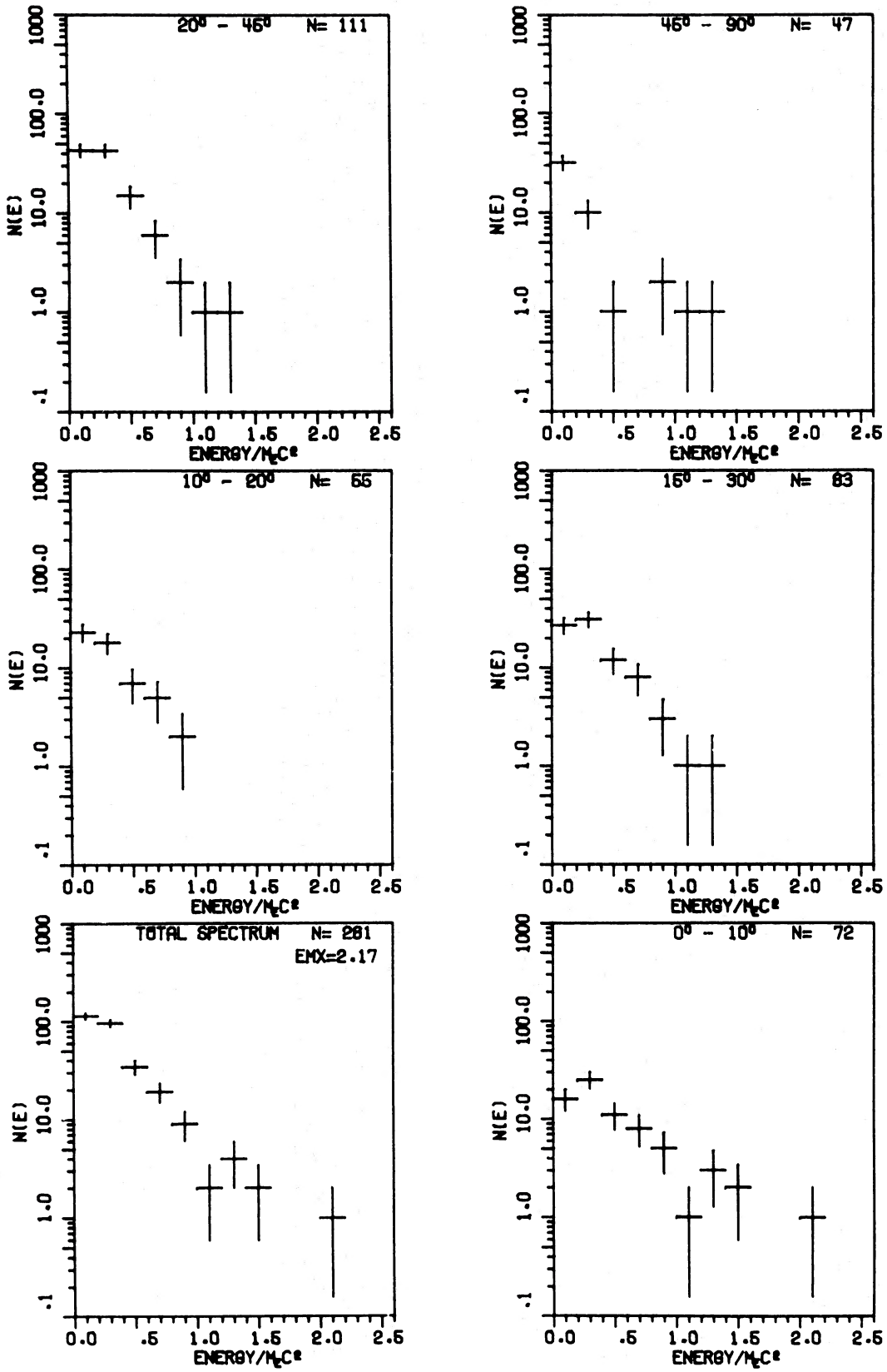


FIG. 3*h*

FIG. 3.—*Continued*



© American Astronomical Society • Provided by the NASA Astrophysics Data System

1977ApJ...214..268P

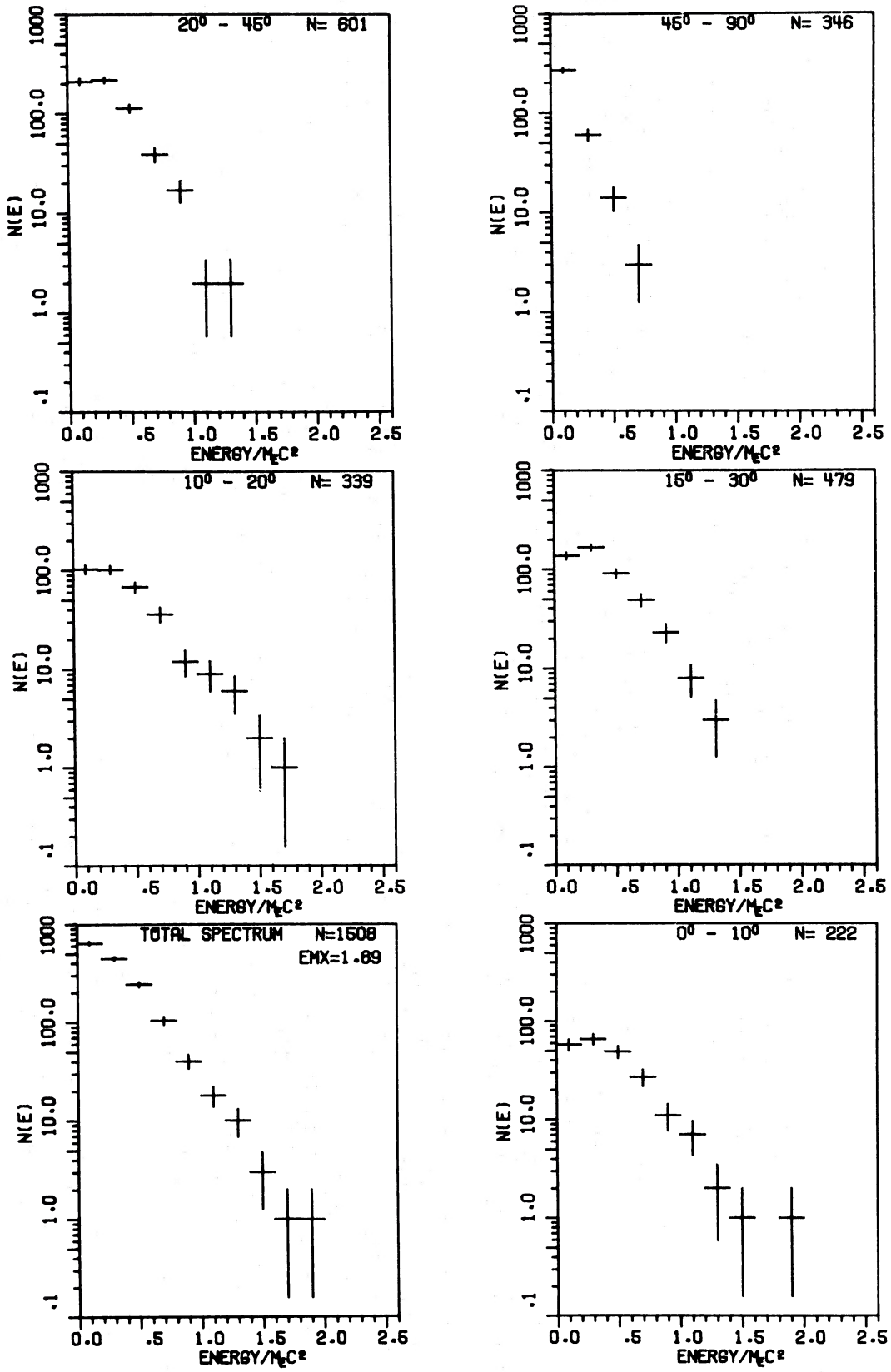


FIG. 3*i*

FIG. 3.—*Continued*



© American Astronomical Society • Provided by the NASA Astrophysics Data System

1977ApJ...214..268P

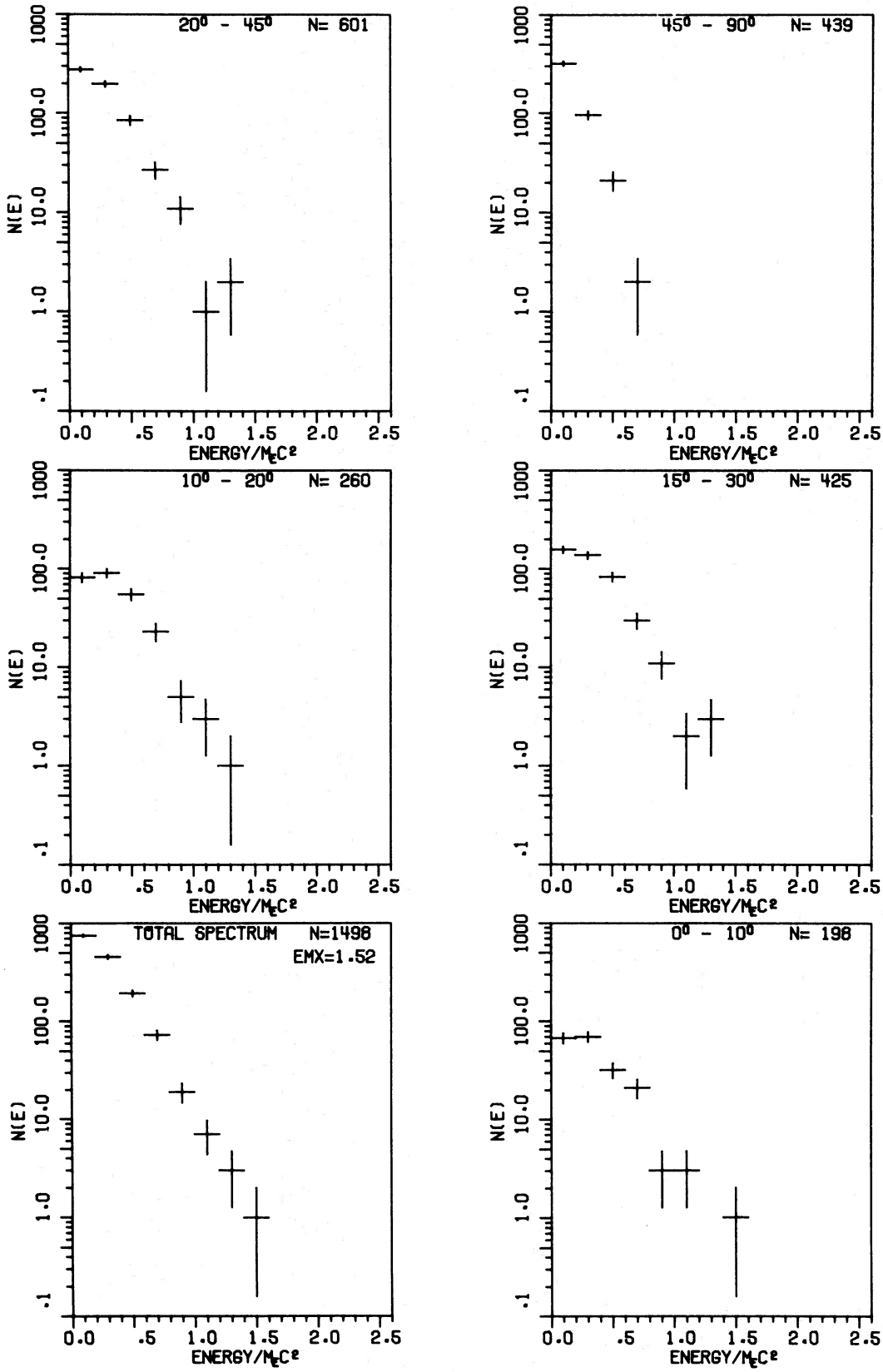


FIG. 3*j*

FIG. 3.—*Continued*



© American Astronomical Society • Provided by the NASA Astrophysics Data System

1977ApJ...214..268P

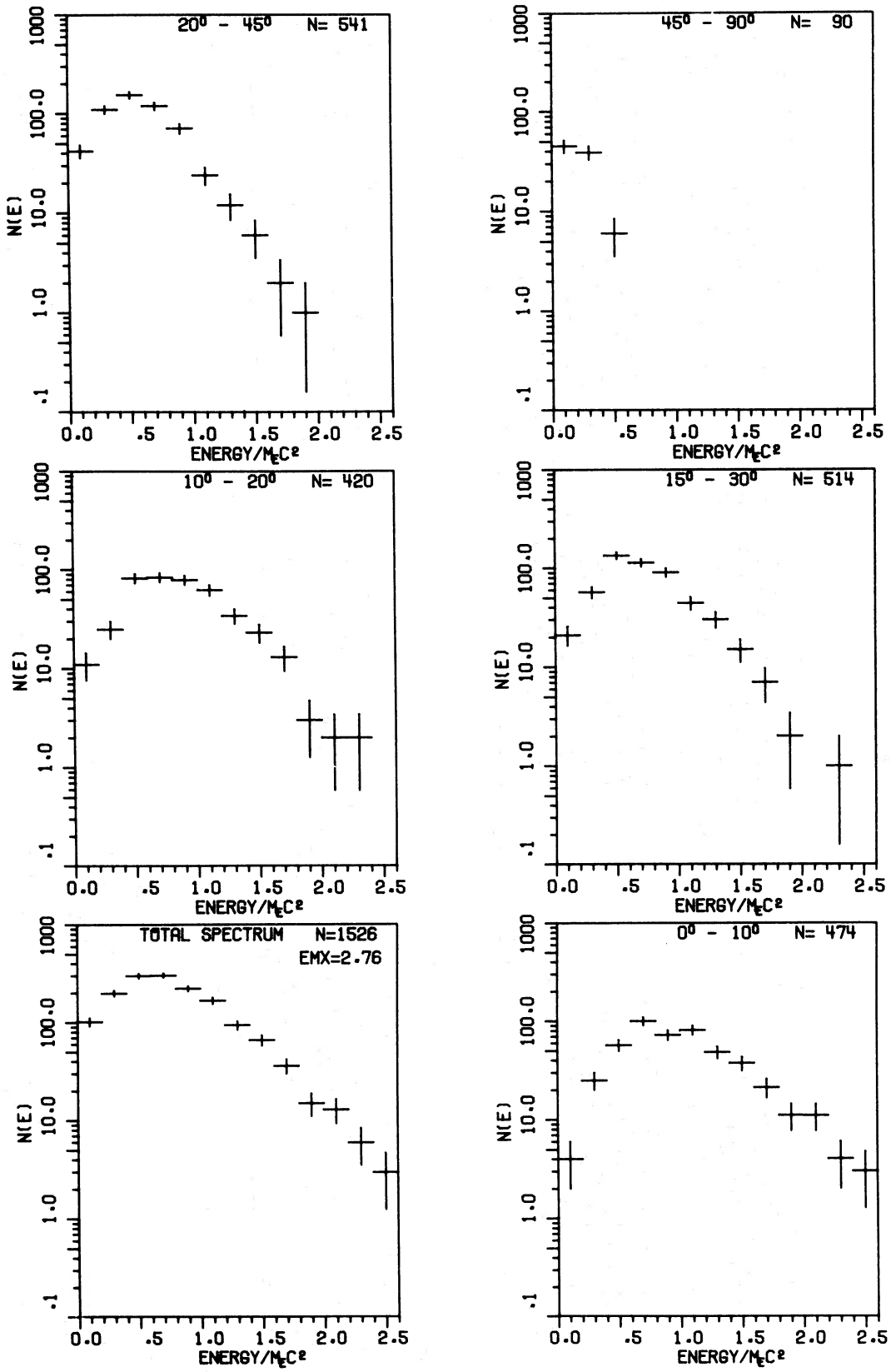


FIG. 3*k*

FIG. 3.—*Continued*



© American Astronomical Society • Provided by the NASA Astrophysics Data System

1977ApJ...214..268P

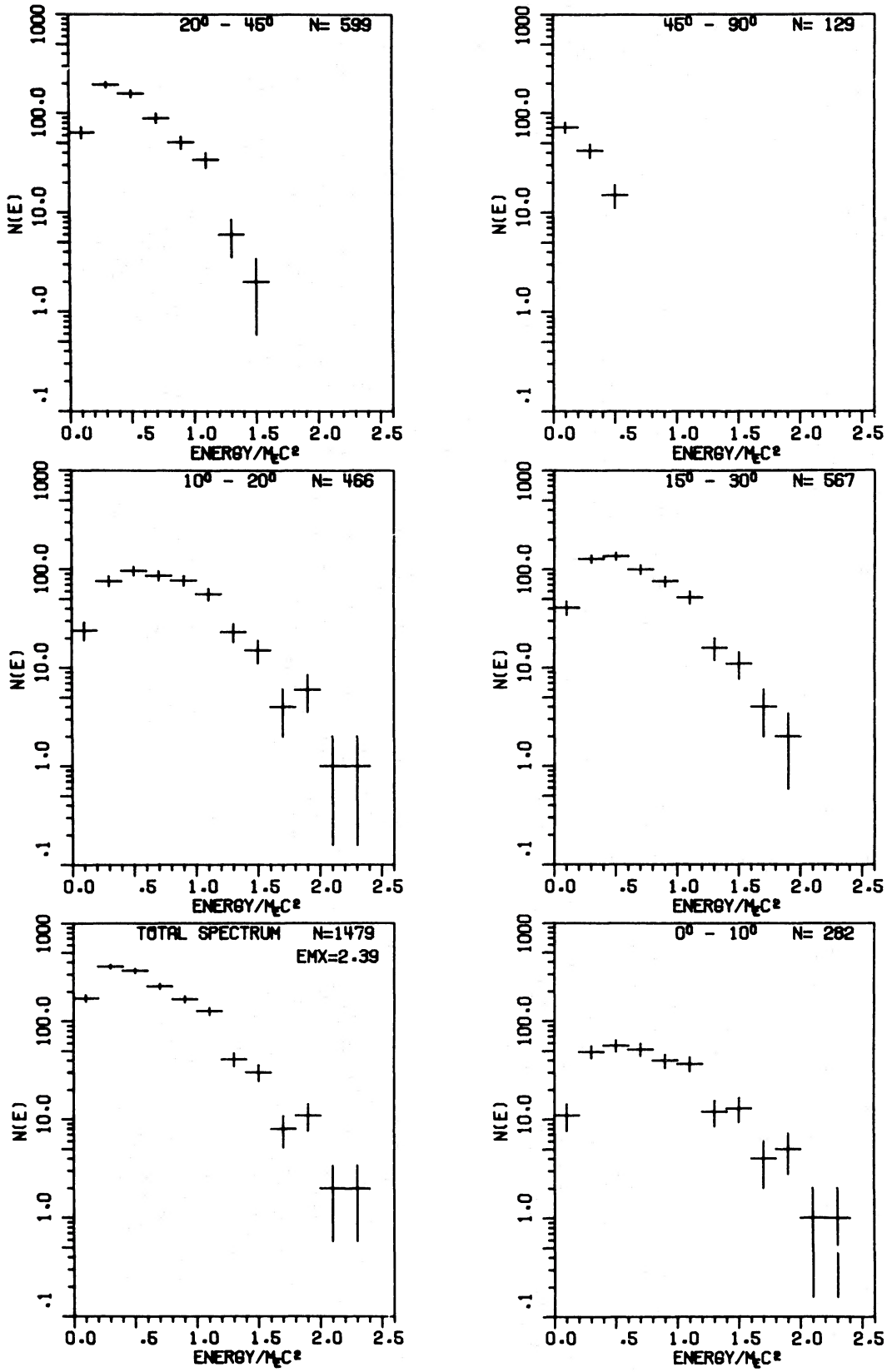


FIG. 3*l*

FIG. 3.—*Continued*



© American Astronomical Society • Provided by the NASA Astrophysics Data System

1977ApJ...214..268P

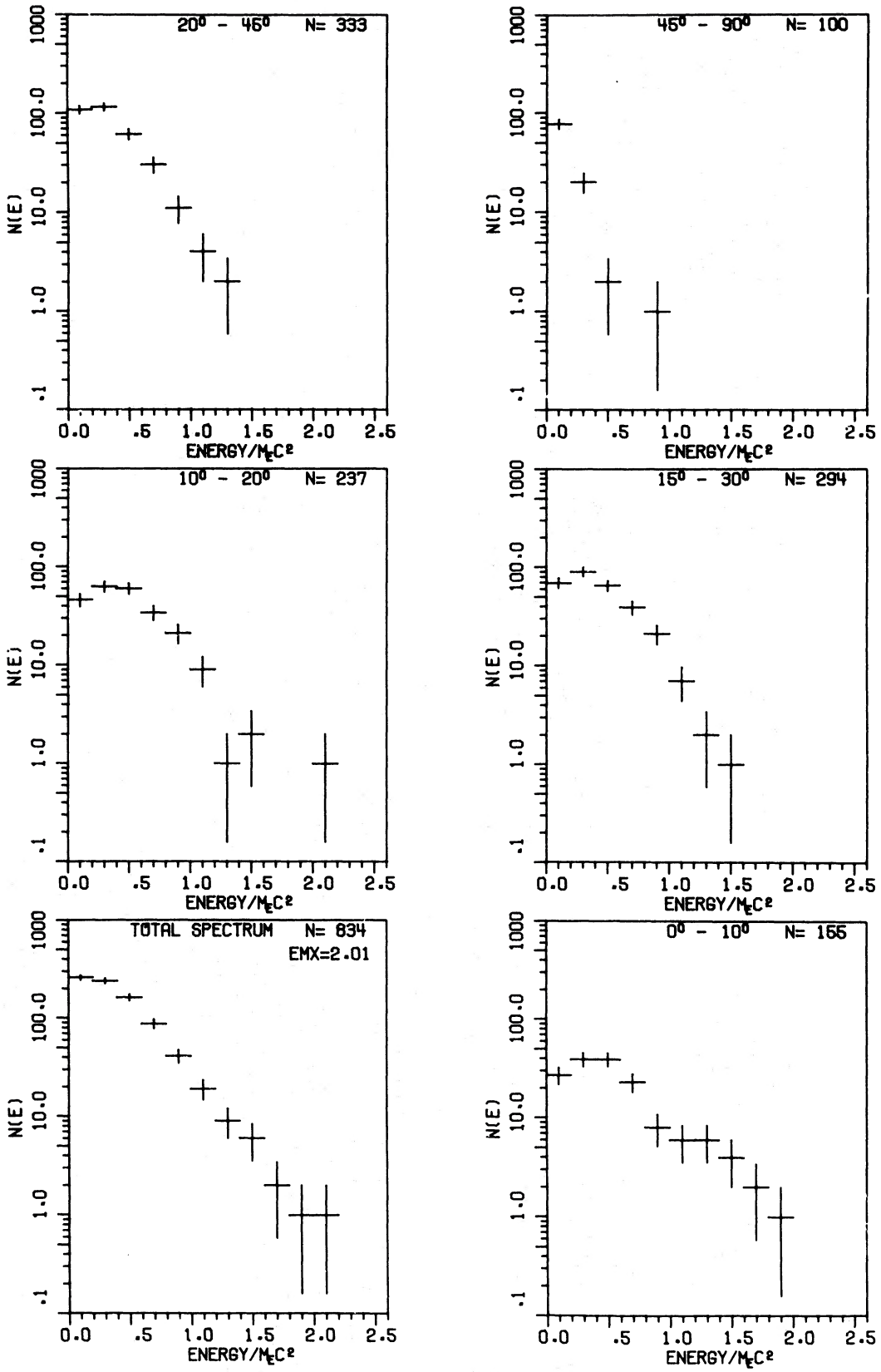


FIG. 3*m*

FIG. 3.—*Continued*



© American Astronomical Society • Provided by the NASA Astrophysics Data System

1977ApJ...214..268P

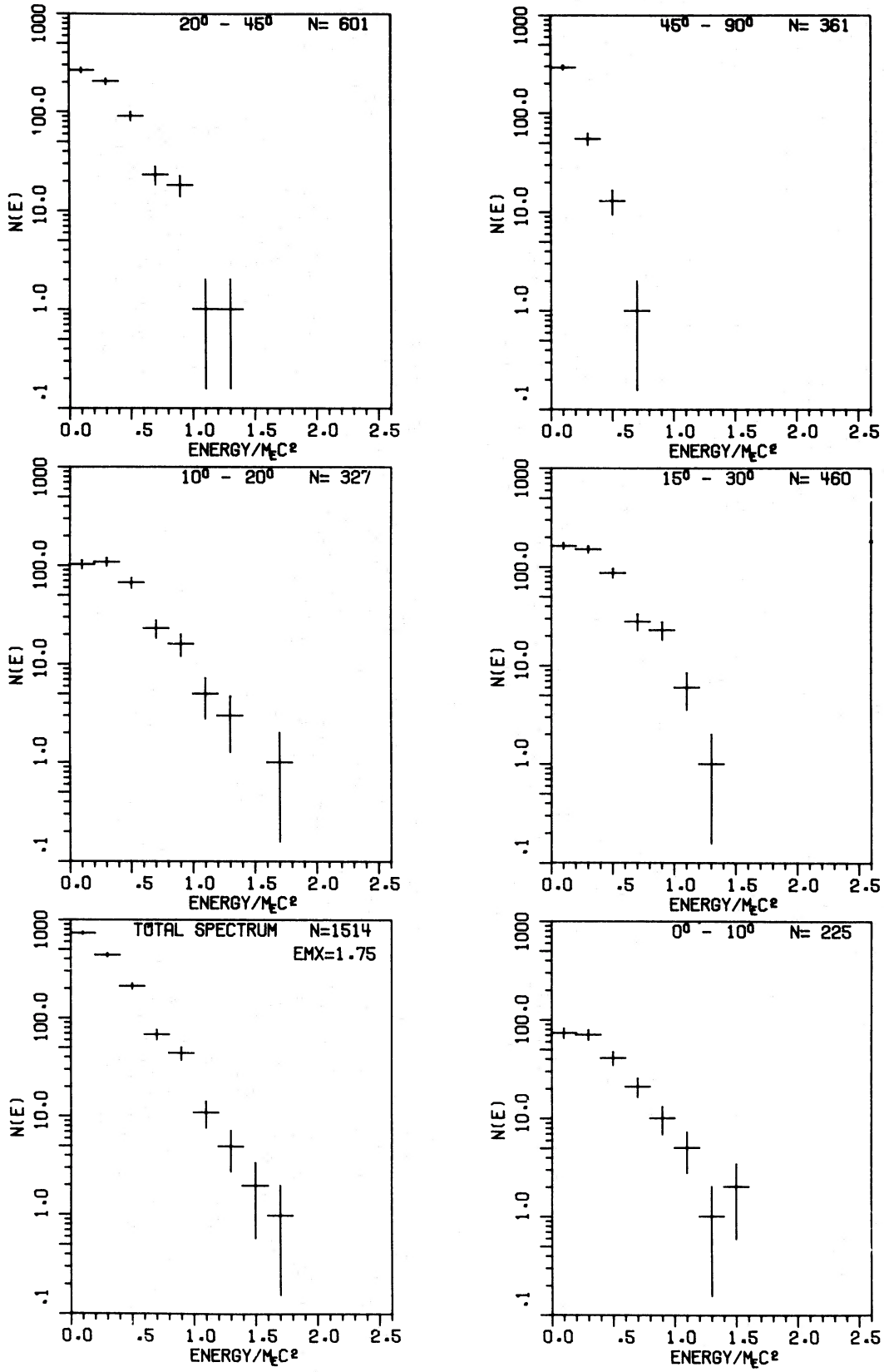


FIG. 3*n*

FIG. 3.—*Continued*



© American Astronomical Society • Provided by the NASA Astrophysics Data System

1977ApJ...214..268P

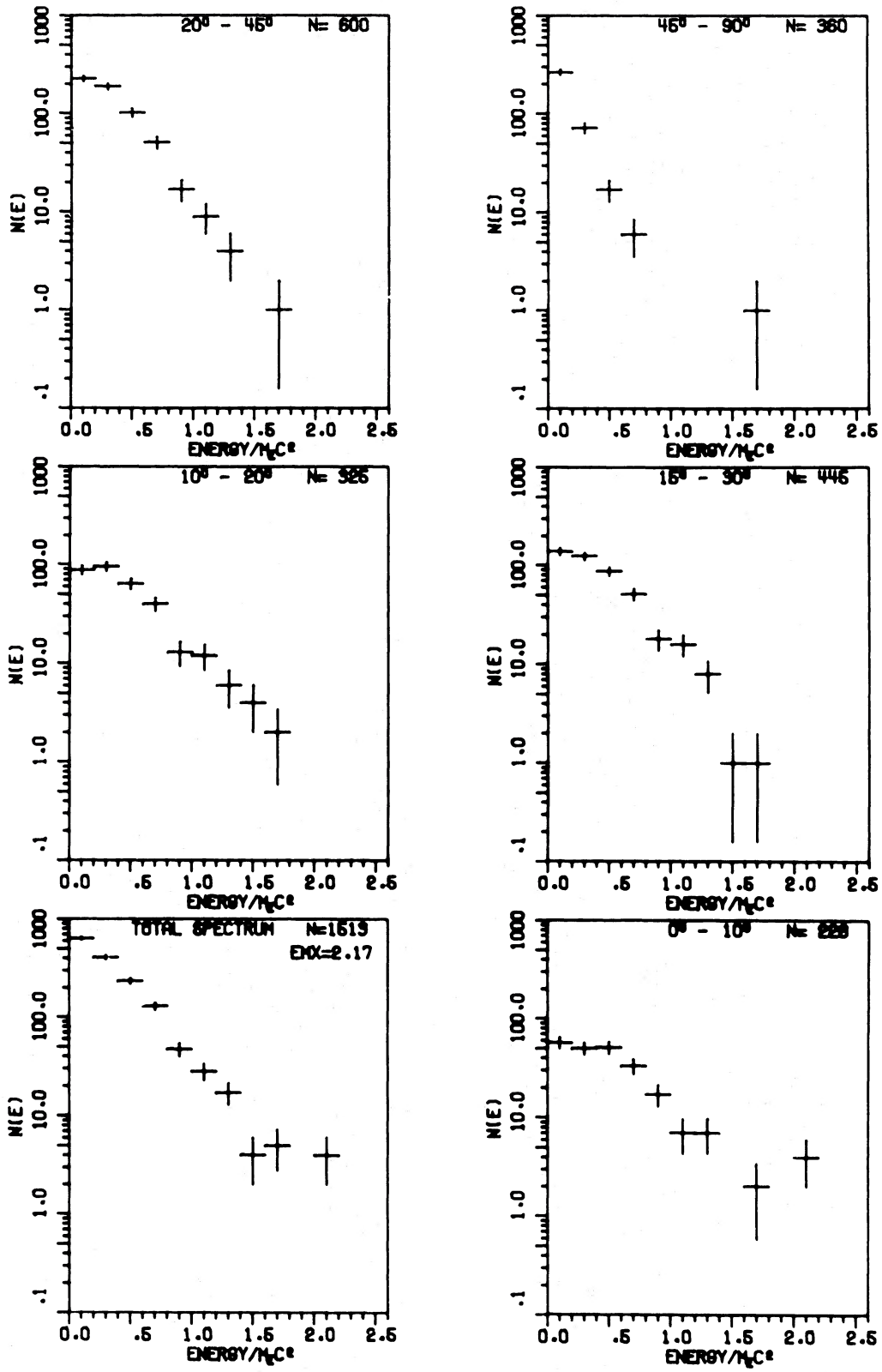


FIG. 3*o*

FIG. 3.—*Continued*



© American Astronomical Society • Provided by the NASA Astrophysics Data System

1977ApJ...214..268P

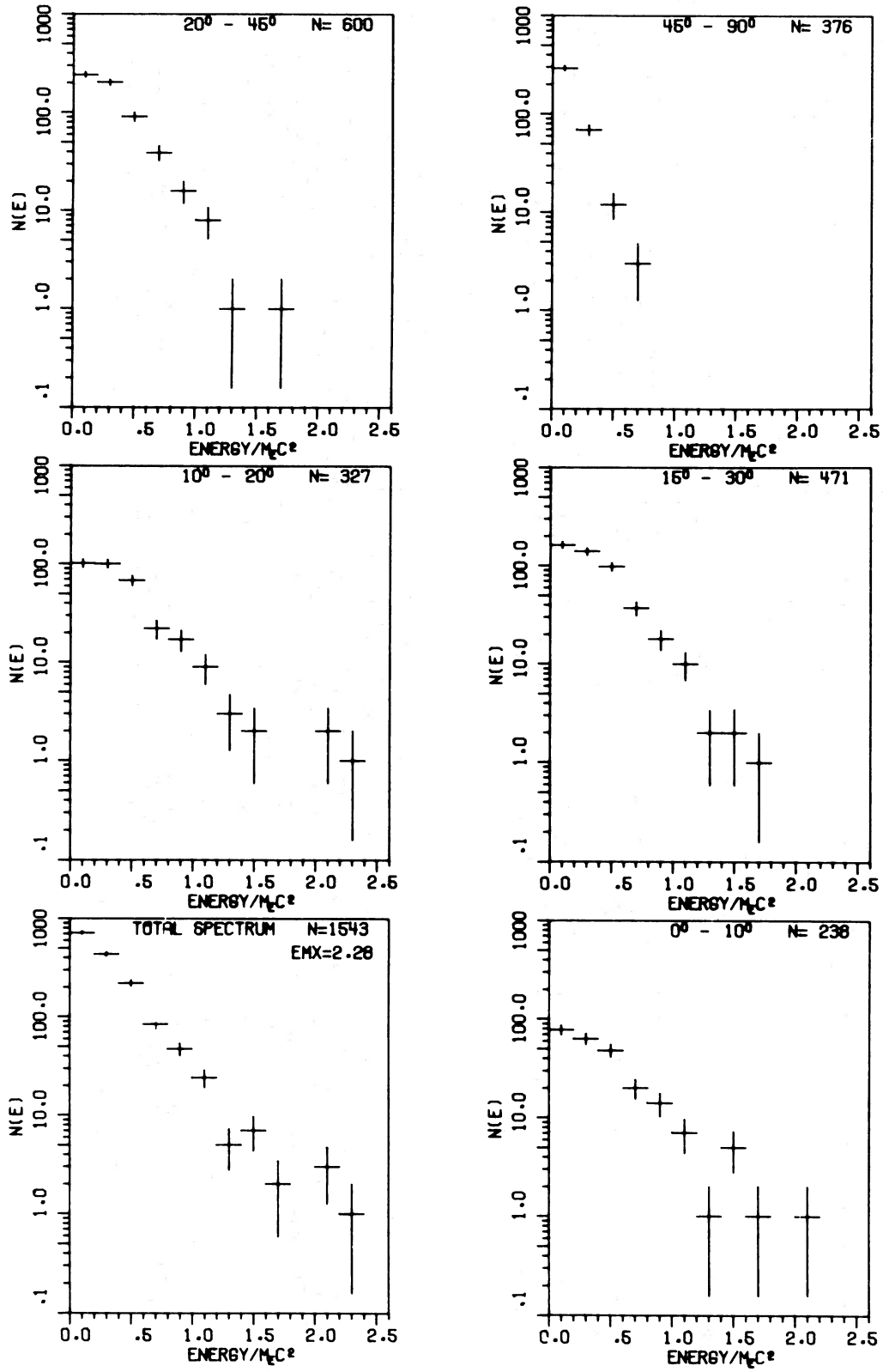


FIG. 3*p*

FIG. 3.—*Continued*



© American Astronomical Society • Provided by the NASA Astrophysics Data System

1977ApJ...214..268P

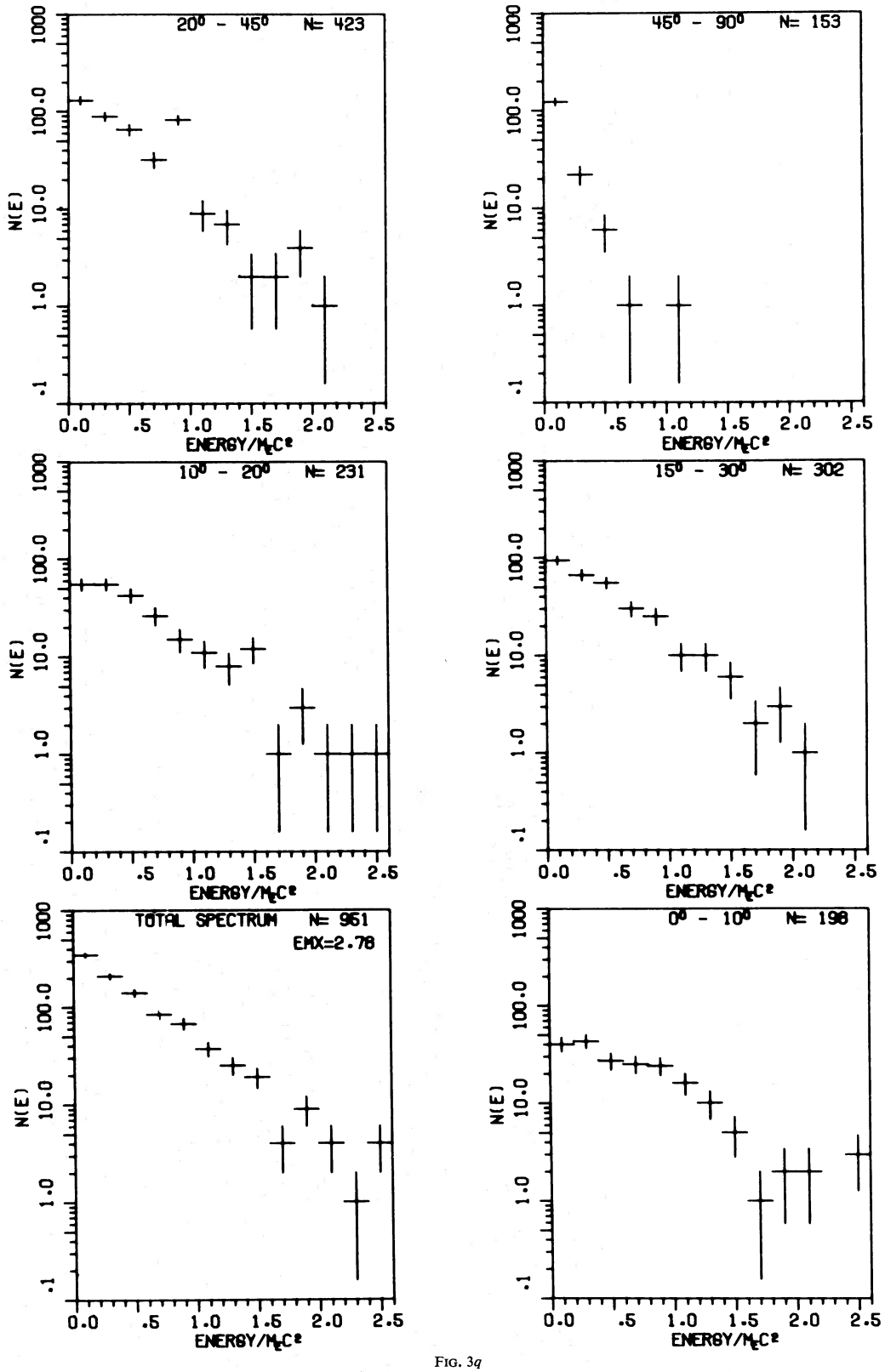


FIG. 3*q*

FIG. 3.—*Continued*



© American Astronomical Society • Provided by the NASA Astrophysics Data System

1977ApJ...214..268P

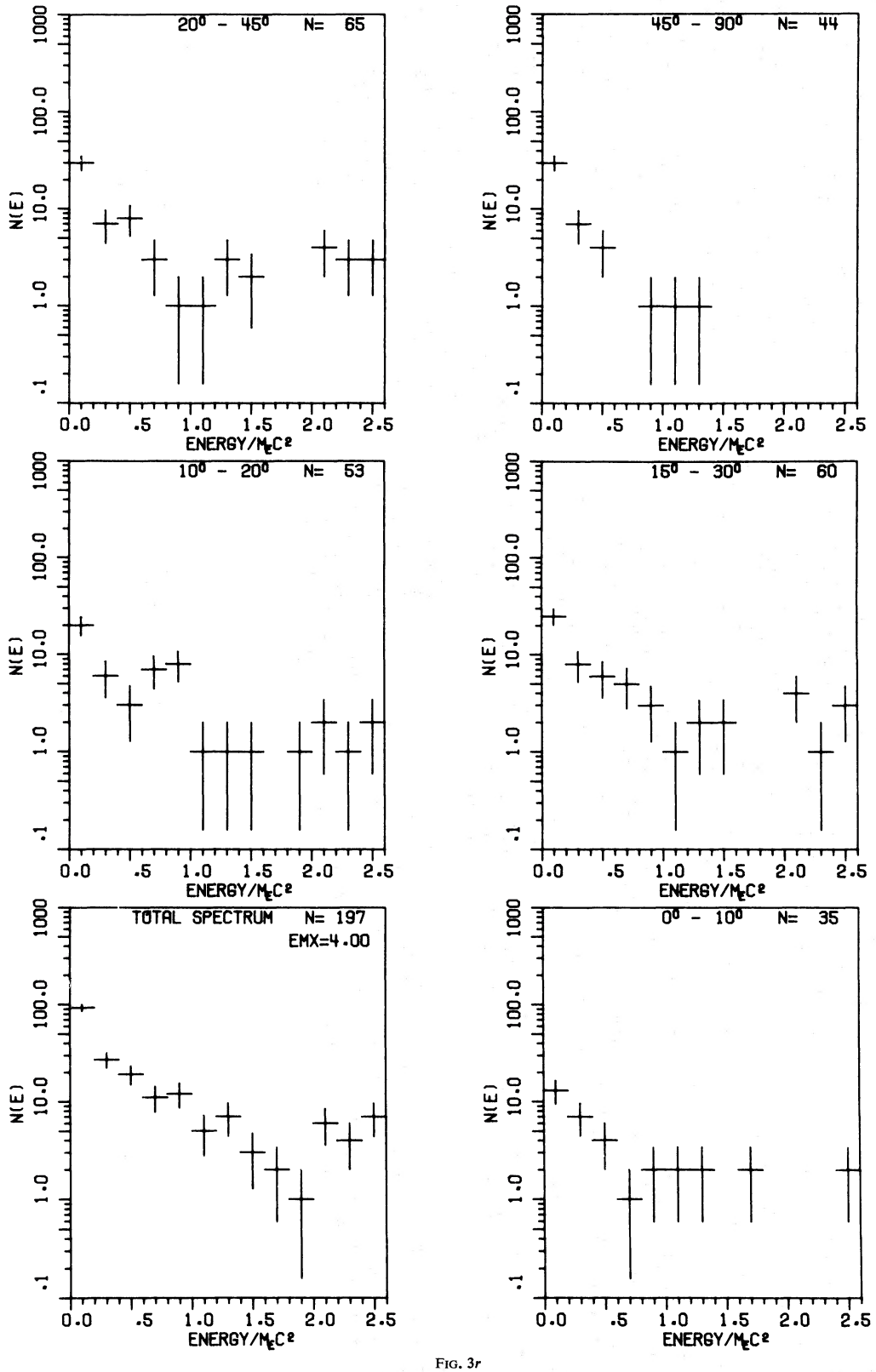


FIG. 3*r*

FIG. 3.—*Continued*



© American Astronomical Society • Provided by the NASA Astrophysics Data System

1977ApJ...214..268P



TABLE 1

SUMMARY OF PARAMETERS FOR FIGURE 3

| Figure | Density Distribution | Velocity Distribution | $T_e$ (Maxwellian) | $T_{ph}$ (blackbody) | $\tau$* | Average Number of Scatterings† | Efficiency‡ | Photon Efficiency§ |
|---|---|---|---|---|---|---|---|---|
| 3*a*..... | Calculated (see Fig. 2) | Calculated | Calculated | 50 keV | 0.1 | 1.03 | 0.13 | 296/7307 |
| 3*b*..... | Calculated | Calculated | Calculated | 50 keV | 0.6 | 1.2 | 0.7 | 616/3172 |
| 3*c*..... | Calculated | Calculated | Calculated | 50 keV | 1.5 | 1.5 | 1.6 | 813/2279 |
| 3*d*..... | Calculated | Calculated | Calculated | 50 keV | 3.0 | 2.2 | 1.6 | 2290/4795 |
| 3*e*..... | Calculated | Calculated | Calculated | 50 keV | 6.0 | 3.6 | 1.8 | 711/1278 |
| 3*f*..... | Calculated | Calculated | Calculated | 50 keV | 12.0 | 6.0 | 1.6 | 784/1406 |
| 3*g*..... | Calculated | Calculated | Calculated | 25 keV | 3.0 | 2.2 | 2.5 | 1385/2599 |
| 3*h*..... | Constant throughout the ergosphere $\pm 10°$ from the equatorial plane | Circular‖ | $10^9$ K | 50 keV | 0.1 | 1.00 | 0.06 | 281/12569 |
| 3*i*..... | Constant throughout the ergosphere $\pm 10°$ from the equatorial plane | Circular | $10^9$ K | 50 keV | 2.5 | 1.83 | 1.4 | 1508/2660 |
| 3*j*..... | Constant throughout the ergosphere $\pm 10°$ from the equatorial plane | Circular | $10^9$ K | 50 keV | 10.0 | 4.41 | 1.7 | 1498/1911 |
| 3*k*..... | Constant between $r_{ms}$ and $r_{mb}$ ($\pm 10°$) | Circular | $10^9$ K | 50 keV | 0.2 | 1.09 | 0.47 | 1526/25000 |
| 3*l*..... | Constant between $r_{ms}$ and $r_{mb}$ ($\pm 10°$) | Circular | $10^9$ K | 50 keV | 2.1 | 2.2 | 2.3 | 1479/3881 |
| 3*m*.... | Constant between $r_{ms}$ and $r_{mb}$ ($\pm 10°$) | Circular | $10^9$ K | 50 keV | 10.0 | 9.5 | 2.3 | 834/1330 |
| 3*n*..... | Constant throughout the ergosphere ($\pm 10°$) | Circular‖ | $5 \times 10^8$ K | 50 keV | 2.6 | 1.8 | 1.3 | 1514/2698 |
| 3*o*..... | Constant throughout the ergosphere ($\pm 10°$) | Circular | $2.5 \times 10^9$ K | 50 keV | 2.6 | 1.8 | 1.5 | 1513/2684 |
| 3*p*..... | Constant throughout the ergosphere ($\pm 30°$) | Circular | $10^9$ K | 50 keV | 2.6 | 3.0 | 1.5 | 1543/2536 |
| 3*q*..... | Calculated# | Calculated# | Calculated# | 50 keV | 1.8 | 2.1 | 1.2 | 951/3054 |
| 3*r*..... | Calculated# | Calculated# | Calculated# | 50 keV | 1.7 | 2.5 | 1.2 | 197/3715 |

* $\tau$ is the optical depth for an average initial photon.

† The average number of scatterings is calculated per scattered photon.

‡ The efficiency stands for the ratio between the total energy of the escaping photons divided by the total energy of the impinging initial photons.

§ Photon efficiency stands for number of escaping photons per total number of initial photons.

‖ The electrons move in spherical orbits, with $P_{e\theta} = 0$, i.e., the electron is in its turning point with respect to the angle relative to the equatorial plane.

# See the text for description of these two distributions.

without being scattered even once. This situation guarantees an efficient use of the initial photon flux; the ratio between the energy flux of the escaping photons to the initial energy flux is 1.6.

When the ergosphere becomes optically thinner, the number of scattered photons, and with it the efficiency, quickly drop. When the system becomes thicker, the number of scatterings does increase, but the spectrum thermalizes. This effect is clearly shown in Figure 3*f*, in which the optical depth was 12.

The effect of thermalization of the spectrum, when the optical depth of the ergosphere is high, is discussed in some detail in Paper I. Detailed calculations of thermal spectra which originate close to the horizon have been performed by Shapiro (1974) for spherical accretion, by Cunningham (1975) for disk configurations, and in Paper I for thermally radiating rings. The main features of such spectra are a characteristic thermal peak in energy (which comes down to lower energies as one observes at higher angles), a general exponential behavior at high energies, and an overall appearance in the equatorial plane similar to spectra emitted from a Newtonian source. The high-energy exponential part of the thermal spectra is in contrast with our Compton spectra, which have, at high energies, a behavior similar to a power law. Furthermore, the thermal spectra are far more sensitive to local plasma temperature than our Compton spectra. The properties of changes in our spectra after variations in the optical depth are also common to other distributions: There are small changes in the shape of the spectrum and decrease in efficiency whenever the optical depth is decreased, and thermalization when the optical path increases. For example, Figures 3*h*–3*j* show the spectra for three different optical depths and for constant density throughout the ergosphere, while Figures 3*k*–3*m* show the same spectra for constant density only in the inner ergosphere.

In the case of a full ergosphere, an electron temperature of about $10^9$ K $\sim$ 100 keV is needed in order to produce a spectrum which resembles the observed ones. When the temperature is lower, as in Figure 3*n*

© American Astronomical Society • Provided by the NASA Astrophysics Data System

1977ApJ...214..268P



(in which the temperature is $5 \times 10^8$ K $\sim$ 50 keV), the resulting spectra are too soft, even though still harder than a thermal spectrum resulting from such a temperature. An increase of the electron temperature to $2.5 \times 10^9$ K, as in Figure 3*o*, does not change the spectrum greatly compared with that of $10^9$ K (in contrast to what, again, would have been the case for thermal processes).

The spectrum of escaping photons also does not change much when the angular width of the disk increases. This is illustrated in Figure 3*p*, where we present the spectrum resulting from scattering from electrons which are distributed uniformly throughout the ergosphere and between $\pm 30°$ from the equatorial plane.

Finally, we present, in Figures 3*q*–3*r*, spectra resulting from scattering by two other calculated distributions. These distributions have a higher initial temperature; hence the matter in these cases is distributed between wider angles ($\pm 40°$ for the distribution used for Fig. 3*q* and almost uniformly in $\Theta$ for Fig. 3*r*). Owing to the higher initial temperature, the resulting final electron temperature is also higher, and reaches a few hundred keV in the inner ergosphere.

The lower part of the spectra (below 300 keV) should also include thermal photons, which originate in the infalling plasma by bremsstrahlung processes. The mechanism for these processes has already been described in detail in connection with steady-state accretion disks. In the configuration that we discuss, the optical depth for free-free processes, $\tau_{\rm ff}$, is much smaller than unity, while the optical depth for electron scattering, $\tau_{\rm es}$, is higher than unity. The parameter which measures the overall optical depth of the system is $\tau^* = (\tau_{\rm es}\tau_{\rm ff})^{1/2}$; and even though $\tau_{\rm es} > 1$, we find $\tau^* < 1$, and the infalling matter is optically thin. In such a case, bremsstrahlung is indeed the dominant radiation mechanism, but the process is very inefficient and the electron temperature is much higher than the temperature of the emitted photons (Novikov and Thorne 1973). Since $\tau_{\rm es} > 1$, the photons will undergo a few scatterings before they leave the plasma. Note that the optical depth for these soft photons is higher than the optical depth of the harder photons which free-fall onto the plasma. These scatterings will not result in Penrose processes, since the photons do not have the needed high energy relative to the electrons, and they can gain only the thermal energy of the electrons. The efficiency of these thermal Compton processes can be measured by the parameter $y$, $y = (4kT_e/\mu_e c^2)\tau^2$ (Lightman, Rees, and Shapiro 1975). In our configuration, $y$ is greater than unity and the Comptonization is efficient; hence the resulting photon spectra should be thermal ones.

The overall spectra that we postulate constitute, therefore, the sum of these two contributions. Variations in the configuration during the instability, in particular variations in the optical depth, will cause rapid changes in the $\gamma$-ray burst spectrum. Since the hard Compton X-rays and the very soft Compton $\gamma$-rays are superposed on those which originate in the thermal processes occurring outside the ergosphere, the softer burst would last longer, and the harder $\gamma$-rays will be seen as riding on a softer burst, which has a longer time span.

## VI. PLASMA RELAXATION

The spectra we have presented in § V were all calculated under the assumption that each photon is scattered by electrons which, although they have a local thermal Maxwellian distribution of velocities, move with the average matter velocity. We can convince ourselves, by a simple order-of-magnitude argument, that actually each electron will scatter many impinging photons in the deep ergosphere before finally disappearing behind the horizon; one should determine how well the average velocity of electrons is restored, after each scattering, to coincide with the overall proton motion.

The order-of-magnitude argument goes as follows: We require optical depths of order unity for the ergosphere. Write $\kappa_{\rm es}\rho r_g \sim \tau$, with $\tau$ the optical depth and where $\rho$ is determined by the accretion rate $\dot{m}$, $\rho c r_g^2 \sim \dot{m}$. Let $\bar{\nu}$ be the average frequency of the X-ray photons produced outside. Clearly, the average infalling photons density in the ergosphere, $n_{\rm ph}$, is determined by $n_{\rm ph} c r_g^2 \sim \eta(\dot{m}c^2/h\bar{\nu})$, where $\eta$ includes the efficiency of rest-mass-to-radiation conversion in the outer region and the solid angle. We estimate $\eta$ to be of order $10^{-2}$. The mean free path $l_e$, for an ergosphere electron in the surrounding photon sea, is now

$$l_e \approx \frac{1}{\mu_p \kappa_{\rm es} n_{\rm ph}} \approx r_g\left(\frac{h\bar{\nu}}{\eta \mu_p c^2 \tau}\right), \qquad (5)$$

where the last estimate was obtained by utilizing the previous equations. By any reasonable model, we must have $h\bar{\nu}/\tau\eta \ll \mu_p c^2$, hence $l_e/r_g \ll 1$ and, indeed, each electron is scattered many times. Note that our estimate (5) shows $l_e$ not to directly depend on the flux of incident X-ray photons. It depends only on their average energy and on the efficiency.

Electron-proton Coulomb collisions alone will not be able to relax the scattered electrons at a sufficiently fast rate, as one may easily verify (on utilizing the book by Spitzer 1962); it turns out that the time to cool the "inverse" Compton heated electron off, in the local inertial frame in which $T_1 \approx 10^{10}$ K, say, is of order $\sim 10^{-3}$–$10^{-4}$ s, much longer than the gravitational time. However, we are not concerned here with equilibrating temperatures; rather, we are concerned with keeping the electron and proton distributions moving at equal average velocities, granting that local "inverse" Compton heating of the electron will occur. Note that the impinging photons increase the local electron energies by increasing their inward radial momentum.

The relevant time scales for the processes that concern us are thus the global plasma relaxation times or diffusion times in the turbulent magnetic field. The growth rate of an electron-proton two-stream instability in this "cold" proton background is given by $\sqrt{3}/2(\mu_e/\mu_p)^{1/3}\omega_{pe}$, where $\omega_{pe}$ is the electron plasma frequency (Stix 1962). In our case, we obtain damping-

© American Astronomical Society • Provided by the NASA Astrophysics Data System

1977ApJ...214..268P



restoring times of order $10^{-13}$ s or somewhat longer; those are indeed small compared with the gravitational or interscattering times. Cyclotron damping times in a possible local magnetic field of $\sim 10^8$ gauss will be of the similar magnitudes. As the individual Compton processes occur at much shorter times ($h/\mu_e c^2$), we see that the electrons have ample time to share their extra linear momentum with the protons between successive Compton scatterings. This shows that the scattered photons do acquire their energy at the expense of the total plasma energy.

Additional dissipation will be caused in the plasma by the restoring mechanisms. The protons will be heated up slightly, and some radiation will be emitted, around the plasma or cyclotron frequencies. This radiation will be mostly captured by the black hole, as it will be mostly emitted radially inward.

## VII. COMPARISON WITH OBSERVATIONS

Two important parameters are measured for the various $\gamma$-ray bursts (Klebesadel, Strong, and Olson 1973); these are $F$, the total energy flux on Earth, and $T$, the burst duration. For various scenarios, one must relate several other parameters to these two quantities.

The total energy radiated by the source, $L_B$, is given by

$$L_B = 4\pi\alpha\, FD^2 = 6\times 10^{37}\left(\frac{\alpha_1}{0.5}\right)\left(\frac{F}{10^{-6}\ \mathrm{ergs\ s^{-1}}}\right)\left(\frac{D}{1\ \mathrm{kpc}}\right)^2 \mathrm{ergs}\,, \tag{6}$$

where $D$ is the distance to the source and $\alpha_1$ is the anisotropy parameter, around 0.5 for our model (as most of the burst energy is radiated in angles less than 45° from the equatorial plane).

The total mass accreted onto the black hole during the burst is therefore

$$M_B = \frac{L_B}{\alpha_2 c^2} = 7\times 10^{16}\left(\frac{\alpha_1}{0.5}\right)\left(\frac{F}{10^{-6}}\right)\left(\frac{D}{1\ \mathrm{kpc}}\right)^2 \frac{1}{\alpha_2}\,\mathrm{g}, \tag{7}$$

where $\alpha_2$ denotes the efficiency of the process in terms of mass-to-energy conversion. Assume that this mass falls into the black hole in $T$ seconds and that, while falling in, it spends a time $\alpha_4 t_g$ in the inner ergosphere ($t_g = r_g/c = 5\times 10^{-6}\ M$ s; $M$ in solar masses). Under these circumstances, we write the optical depth throughout the ergosphere as

$$\tau \approx \kappa_{\mathrm{es}}\frac{\alpha_4 t_3}{T}\cdot\frac{M_B}{4\pi\alpha_3 r_g{}^2} \approx 2\times 10^{-2}\left(\frac{\alpha_1}{0.5}\right)\left(\frac{F}{10^{-6}}\right)\left(\frac{D}{1\ \mathrm{kpc}}\right)^2 \times\left(\frac{6\ \mathrm{s}}{T}\right)\left(\frac{10}{M}\right)\left(\frac{0.5}{\alpha_3}\right)\frac{\alpha_4}{\alpha_2}\,, \tag{8}$$

where $\alpha_3$ is the height-to-radius ratio for the innermost disk region. In equation (8) we have used the average Klein-Nishina $\kappa_{\mathrm{es}}$ value in our calculations, $\langle\kappa_{\mathrm{es}}\rangle \approx 0.2$.

The quantity $\alpha_2$ depends primarily on the number of scatterings per electron of the infalling flux of X-ray photons; it also depends on the coupling between protons and electrons, but, as we have seen, this coupling occurs via macroscopic plasma or hydromagnetic modes, and is very efficient. To an observer at infinity, each Compton process reduces the plasma energy by some $0.2\ \mu_e c^2$ (recall that about half of the Compton processes result in trapped photons). Thus, $\alpha_2$ is determined by

$$\alpha_2 \approx \frac{\alpha_4 r_g \mu_e}{5 l_e \mu_p} = 0.5\left(\frac{\alpha_4}{2}\right)\left(\frac{\tau}{5}\right)(50\eta^*)\,, \tag{9}$$

where $l_e$ is given by equation (5), and on defining

$$\eta^* \equiv \eta\,\frac{\mu_e c^2}{5h\bar{\nu}} = 0.02\left(\frac{\eta}{10^{-2}}\right)\left(\frac{h\bar{\nu}}{50\ \mathrm{keV}}\right)^{-1}. \tag{10}$$

We shall normally adopt a value of 0.02 for $\eta^*$, but one should keep in mind that this value could vary for different scenarios.

On substituting equation (9) into (8), we derive

$$\tau \approx \left(\frac{\alpha_1}{0.5}\right)^{1/2}(50\,\eta^*)^{-1/2}\left(\frac{F}{10^{-6}}\right)^{1/2}\left(\frac{D}{1\ \mathrm{kpc}}\right)\left(\frac{10}{M}\right)^{1/2} \times\left(\frac{0.5}{\alpha_3}\right)^{1/2}\left(\frac{6\ \mathrm{s}}{T}\right)^{1/2}. \tag{11}$$

As we have shown previously (see also Paper I), a necessary condition for the process to occur is $\tau \sim 3$. Yet, during the burst, we might have $\langle\tau\rangle \sim 10$. On inverting equation (11) to solve for $D$, we find

$$D = 5\left(\frac{\tau}{5}\right)\left(\frac{0.5}{\alpha_1}\right)^{1/2}(50\,\eta^*)^{1/2}\left(\frac{F}{10^{-6}}\right)^{-1/2}\left(\frac{M}{10}\right)^{1/2} \times\left(\frac{\alpha_3}{0.5}\right)^{1/2}\left(\frac{T}{6\ \mathrm{s}}\right)^{1/2}\mathrm{kpc}\,. \tag{12}$$

Using equations (12), (9), and (7), we rewrite the equation for $M_B$ as

$$M_B = 9\times 10^{18}\left(\frac{\alpha_3}{0.5}\right)\left(\frac{\alpha_4}{2}\right)^{-1}\left(\frac{\tau}{5}\right)\left(\frac{M}{10}\right)\left(\frac{T}{6\ \mathrm{s}}\right)\mathrm{g}\,, \tag{13}$$

and, for the total luminosity, obtain

$$L_B = 1.6\times 10^{39}(50\,\eta^*)\left(\frac{\alpha_3}{0.5}\right)\left(\frac{\tau}{5}\right)^2\left(\frac{M}{10}\right)\left(\frac{T}{6\ \mathrm{s}}\right)\mathrm{ergs\ s^{-1}}. \tag{14}$$

It should be noted that, by equations (13) and (14), our model eliminates the dependence on $F$ and depends only on $T$. However, it does contain some uncertainties, in particular with respect to $\eta^*$.

© American Astronomical Society • Provided by the NASA Astrophysics Data System

1977ApJ...214..268P



We might also try to estimate $\rho$, from $\tau \approx 0.2\rho r_g$. We obtain

$$\rho \approx 10^{-5}\left(\frac{\tau}{5}\right)\left(\frac{M}{10}\right)^{-1} \text{ g cc}^{-1}. \quad (15)$$

In the case of a possible burst coming from the X-ray source Cyg X-1, the values calculated from equations (12)–(14) can be compared with the quantities measured for the X-ray source using its steady-state X-ray and optical data. Recent reviews of the optical properties of Cyg X-1 by Bahcall (1975) and of its X-ray data by Giacconi (1975) estimate the mass of the compact object in Cyg X-1 to be $9 < M < 25$ if the system is not a triple-star system. (Note, again, that we measure $M$ in solar masses.) The distance to this system is about 2 kpc (see also Margon, Bowyer, and Stone 1973; Paczyński 1974; Cheng, Phillips, and Wilson 1974). The intensity of the X-ray emission depends on the state of the source, and it ranges between $2 \times 10^{37}$ ergs s$^{-1}$ in the high state to $5 \times 10^{36}$ ergs s$^{-1}$ in the low state. There is no eclipse in the X-rays; hence it is clear that we are at some angle to the plane in which the components of the system move. It is reasonable to assume that this plane is also the plane of the disk and the equatorial plane of the black hole (Bardeen and Petterson 1975). On the other hand, since there are some periodical variations in the X-ray intensity (Holt *et al.* 1976), we are most likely not at a very high angle relative to this plane. An acceptable estimate for our angle is 30° from the plane—a very convenient angle for $\gamma$-rays, by our model.

The measured values of $F$ and $T$ for a burst which is possibly coming from the direction of Cyg X-1 are $5 \times 10^{-5}$ ergs cm$^{-2}$ and 6 s (Strong 1976). Substituting these values in equation (12), along with $M = 15$ and the "nominal" values for the parameters $\alpha_1$ and $\alpha_3$, yields $D \approx (50\,\eta^*)^{1/2}$ kpc. Such a value would be consistent with the 2 kpc distance accepted for Cyg X-1 if $\eta^* \sim 8 \times 10^{-2}$ and $M_B \approx 1.4 \times 10^{19}$ g.

From the steady state for $L_x$ value one may estimate $\dot{m}$ to be $1.2 \times 10^{17}$ g s$^{-1}$. Using the formulae for disk structure (Novikov and Thorne 1973), with these values for $M$ and $\dot{m}$, and with a value of 0.1 for the viscosity parameter, $\alpha$, one verifies that indeed some $10^{19}$ g are contained in the six inner gravitational radii of the disk, which is about the size of the inner unstable region. During the steady-state accretion, the matter drifts along this distance in 200 s (Novikov and Thorne 1973), while the free-fall time from this distance is about $6 \times 10^{-4}$ s. The burst duration, which is 6 s, is just between these two values, thus being consistent with the general picture of a fast hydrodynamic collapse, but not free fall, of the matter in this region into the black hole, with one or two possible perihelion passages in the deep ergosphere to account for occasional multiple structure of the bursts.

One notes that other known data on Cyg X-1 further support the assumption that it could be a source of $\gamma$-ray bursts. For example, Holt *et al.* (1976) suggest that some observations in X-rays, which were done by *Ariel 5*, can be explained if there were a gradual increase in the amount of matter exchanged between the components of the binary system prior to the transition in the X-ray spectrum, and this increase stopped after the change took place. This effect is consistent with a picture of a gradual filling up of the Roche lobe of the primary and a sudden emptying of it, followed by the change to the other state of the disk (Thorne and Price 1975). Some other evidence which supports our model was mentioned in the discussion of the observational properties of $\gamma$-ray bursts.

Other sources of $\gamma$-ray bursts, for which we have known directions at hand, have not been identified with known X-ray sources. (However, note that the error box for burst 72-4 contains a weak and uncataloged X-ray source which was measured by *Uhuru*; Strong 1976.) Yet it is still probable that these sources are binary systems, having a rotating black hole as one component, which satisfy all the requirements of our model, but which, because of a low mass-transfer rate (below $10^{-10}\,M$ per year), have most of their X-ray emission in the soft X-ray regime (Shakura and Sunyaev 1973). Owing to interstellar absorption, such sources are not detected even when they are relatively close to us. Such a low mass-transfer rate could result from stellar wind accretion (Illarionov and Sunyaev 1975), with or without formation of a disk, and it is clear that under such conditions, a burst in the primary would result in large changes in the accretion. The distances to these sources will vary, according to equation (12), from a few tens to a few hundreds of parsecs. There is no clear estimate for the number of black holes in binary systems that could exist in such region, but if we use the estimates of Lamb, Lamb, and Pines (1973) for the number of neutron stars in binary systems that do not emit X-rays in such a region, we can see that it is possible to have a sufficient number of similar systems which contain a black hole to explain the observed number of $\gamma$-ray sources. The distances to most of the sources, calculated using equation (12), are smaller than the distance to Cyg X-1, and this is clearly in agreement with the picture by which Cyg X-1 has a much larger accretion disk than the average $\gamma$-ray burst source; hence the total energy emitted during its bursts is much higher.

As a conclusion for this section, we shall briefly summarize our interpretation for the temporal structure of the bursts.

The duration of the burst is determined by the time of collapse of the inner disk. This time is larger than the free-fall time but smaller than the time of steady-state drift along this region. The exact duration, as well as other details of the temporal structure, can be evaluated only after developing a hydrodynamic or magnetohydrodynamic model, which includes a detailed picture of the viscosity. The quick changes and the microbursts which occur during the burst could be caused by local variations of the optical depth during the burst. The duration of the microburst—the shortest of them is 4 ms (by K. Brecher, private communication)—gives an upper limit of some

© American Astronomical Society • Provided by the NASA Astrophysics Data System

1977ApJ...214..268P



1200 km for the source of the burst, clearly in agreement with our very compact source. However, one might observe microbursts as short as the light travel time over one magnetic blob, which is a few microseconds.

## VIII. CONCLUSION—FURTHER TESTS

With the present observational tools for detection of $\gamma$-ray bursts, it is very difficult to perform further observations which will verify our model. However, in the future, large improvements are expected in these measurements. The following observations would support our model: A verification of the connection between Cyg X-1 and some of the $\gamma$-ray bursts by precise identification of the direction of the $\gamma$-ray burst source; detection of many low-intensity bursts and, in particular, detection of weak bursts of hard X-rays and very soft $\gamma$-rays (which would result from sources with high inclination angle to us); detection of fast changes in the bursts down to a few tens or a few hundred microseconds which will limit the size of the sources to a few kilometers; and detection of steady-state X-ray sources, mainly very soft ones, within the error boxes of the sources of $\gamma$-ray bursts. All of these measurements could give a qualitative support to our model; however, a direct measurement of a third parameter—the distance of the sources, for example—which is impossible now, will enable us to have a direct check.

A confirmation of the possible constancy of the high-energy part of observed spectra would probably be the most important clue, as temperatures of thermal radiation should vary more than the electron mass in such models. Note that, by equation (14), a strong dependence of $L_B$ on the spectrum, via $\tau$, is predicted. This may lead to a correlation between luminosities and observed spectra.

Finally, we note that, in the case of possible bursts from Cyg X-1, our spectrum calculations would imply an orbit inclination angle of about 30° or less relative to us. An independent estimate on that from models for the steady-state X-ray and optical radiation will provide an important consistency check.

It is a pleasure to thank A. P. Lightman for many helpful discussions.

## REFERENCES


Bahcall, J. N. 1975, Lecture, Enrico Fermi Summer School, Varenna, Italy.
Bardeen, J. M. 1970, *Nature*, **226**, 64.
Bardeen, J. M., and Petterson, J. 1975, *Ap. J.* (*Letters*), **195**, L65.
Bardeen, J. M., Press, W. H., and Teukolsky, S. A. 1972, *Ap. J.*, **178**, 347.
Bewick, A., Coe, M. J., Mills, J. S., and Queuby, J. J. 1975, *Nature*, **258**, 686.
Cheng, C. C., Phillips, K. J. H., and Wilson, A. M. 1974, *Nature*, **251**, 589.
Christodoulou, D. 1970, *Phys. Rev. Letters*, **25**, 1596.
Cline, T. L. 1974, *Ann. NY Academy of Sciences*, **262**, 159.
Cline, T. L., and Desai, U. D. 1975, *Ap. J.* (*Letters*), **196**, L43.
Cunningham, C. T. 1975, preprint.
Giacconi, R. 1975, Lecture, Enrico Fermi Summer School, Varenna, Italy.
Grindlay, J. E., Wright, E. L., and McCrosky, R. E. 1974, *Ap. J.* (*Letters*), **192**, L133.
Holt, S. S., Boldt, E. A., Serlemitsos, P. J., and Kaluzienski, L. J. 1976, *Ap. J.* (*Letters*), **203**, L63.
Illarionov, A. F., and Sunyaev, R. A. 1975, *Astr. Ap.*, **39**, 185.
Imhof, W. L., Nakano, G. H., Johnson, R. G., Kilner, J. R., Reagan, J. B., Klebesadel, R. W., and Strong, I. B. 1974, *Ap. J.* (*Letters*), **191**, L7.
Klebesadel, R. W., Strong, I. B., and Olson, R. A. 1973, *Ap. J.* (*Letters*), **182**, L85.
Kovetz, A., and Piran, T. 1975*a*, *Lettere Nuovo Cimento*, **12**, 39.
———. 1975*b*, *Lettere Nuovo Cimento*, **12**, 560.
Lamb, D. Q., Lamb, F. K., and Pines, D. 1973, *Nature Phys. Sci.*, **246**, 52.
Lightman, A. P. 1974*a*, *Ap. J.*, **194**, 419.
———. 1974*b*, *Ap. J.*, **194**, 429.
Lightman, A. P., and Eardley, D. M. 1974, *Ap. J.* (*Letters*), **187**, L1.
Lightman, A. P., Rees, M. J., and Shapiro, S. 1975, Lecture, Enrico Fermi Summer School, Varenna, Italy.
Lin, D. N. C., and Pringle, J. E. 1975, in *IAU Symposium No. 73, The Structure and Evolution of Close Binary Systems*, ed. P. Eggleton, S. Mitton, and J. Whelan (Dordrecht: Reidel).
Margon, B., Bowyer, S., and Stone, R. P. S. 1973, *Ap. J.* (*Letters*), **185**, L113.
Mashhoon, B. 1973, *Ap. J.* (*Letters*), **181**, L65.
Mészáros, P., and Rees, M. J. 1975, *Bull. AAS*, **7**, 242.
Metzger, A. E., Parker, R. H., Gilman, D., Peterson, L. E., and Trombka, J. I. 1974, *Ap. J.* (*Letters*), **194**, L19.
Novikov, I. D., and Thorne, K. S. 1973, in *Black Holes*, ed. C. DeWitt and B. S. DeWitt (New York: Gordon & Breach), p. 343.
Novikov, I. D., and Zel'dovich, Ya. B. 1966, *Nuovo Cimento Suppl.*, **4**, 810.
Paczyński, B. 1974, *Astr. Ap.*, **34**, 161.
Page, D., and Thorne, K. S. 1974, *Ap. J.*, **191**, 499.
Palumbo, G. G. C., Pizzichini, G., and Vespignani, G. R. 1974, *Ap. J.* (*Letters*), **189**, L9.
Penrose, R. 1969, *Rev. Nuovo Cimento*, **1**, 252.
Piran, T., and Shaham, J. 1975*a*, *Nature*, **256**, 112.
———. 1975*b*, Lecture, Enrico Fermi Summer School, Varenna, Italy.
———. 1977, *Phys. Rev.*, in press.
Piran, T., Shaham, J., and Katz, J. 1975, *Ap. J.* (*Letters*), **196**, L107.
Pringle, J. E., and Rees, M. J. 1972, *Astr. Ap.*, **21**, 1.
Pringle, J. E., Rees, M. J., and Pacholzyk, A. G. 1973, *Astr. Ap.*, **29**, 179.
Ruderman, M. 1974, *Ann. NY Academy of Sciences*, **262**, 164.
Sanford, P. W., Ives, J. C., Bell Burnell, S. J., Mason, K. O., and Murdin, P. 1975, *Nature*, **256**, 109.
Shakura, N. T., and Sunyaev, R. A. 1973, *Astr. Ap.*, **24**, 337.
Shapiro, S. L. 1974, *Ap. J.*, **189**, 343.
Shapiro, S. L., and Lightman, A. P. 1975, preprint.
Shapiro, S. L., Lightman, A. P., and Eardley, D. M. 1976, preprint.
Shklovsky, I. S. 1967, *Ap. J.* (*Letters*), **148**, L1.
Spitzer, L. J. R. 1962, *Physics of Fully Ionized Gases* (New York: Wiley).
Stix, T. H. 1962, *The Theory of Plasma Waves* (New York: McGraw-Hill).
Strong, I. B. 1976, private communication.
Strong, I. B., and Klebesadel, W. R. 1974, *Nature*, **251**, 396.
Strong, I. B., Klebesadel, W. R., and Evans, W. D. 1974, *Ann. NY Academy of Sciences*, **262**, 145.
———. 1975, Lecture, Enrico Fermi Summer School, Varenna, Italy.
Tananbaum, H., Gursky, H., Kellogg, E., Giacconi, R., and Jones, C. 1972, *Ap. J.* (*Letters*), **177**, L5.


© American Astronomical Society • Provided by the NASA Astrophysics Data System

1977ApJ...214..268P



Tananbaum, H., and Hutchings, J. B. 1974, *Ann. NY Academy of Sciences*, **262**, 299.
Thorne, K. S. 1974, *Ap. J.*, **191**, 507.
Thorne, K. S., and Price, R. H. 1975, *Ap. J. (Letters)*, **195**, L101.
van den Heuvel, E. P. J. 1975, Lecture, Enrico Fermi Summer School, Varenna, Italy.
Wald, R. M. 1974, *Ap. J.*, **191**, 231.
Wheaton, W. A., Ulmer, M. P., Baity, W. A., Datlowe, D. W., Elcan, M. J., Peterson, L. E., Klebesadel, R. W., Strong, I. B., Cline, T. L., and Desai, U. D. 1973, *Ap. J. (Letters)*, **185**, L57.

TSVI PIRAN: Department of Astrophysics, Oxford University, South Parks Road, Oxford OX1 3RQ, England
JACOB SHAHAM: Racah Institute of Physics, Hebrew University, Jerusalem, Israel

© American Astronomical Society • Provided by the NASA Astrophysics Data System